5-1-2015

Carbon Isotope Variations Associated with a Middle Ordovician Karstic Unconformity

Patricia Suzanne Williams
University of Nevada, Las Vegas

CARBON ISOTOPE VARIATIONS ASSOCIATED WITH A MIDDLE ORDOVICIAN KARSTIC UNCONFORMITY

By

Patricia Suzanne Williams

Bachelor of Science in Geology and Geophysics

Missouri University of Science and Technology

2012

A thesis submitted in partial fulfillment

of the requirements for the

Master of Science - Geoscience

Department of Geoscience

College of Science

The Graduate College

University of Nevada, Las Vegas

May 2015

UNLV | GRADUATE COLLEGE

We recommend the thesis prepared under our supervision by

Patricia Suzanne Williams

entitled

Carbon Isotope Variations Associated with a Middle Ordovician Karstic Unconformity

is approved in partial fulfillment of the requirements for the degree of

Master of Science - Geoscience

Department of Geosciences

Ganqing Jiang, Ph.D., Committee Chair

Terry Spell, Ph.D., Committee Member

Minghua Ren, Ph.D., Committee Member

Brian Hedlund, Ph.D., Graduate College Representative

Kathryn Hausbeck Korgan, Ph.D., Interim Dean of the Graduate College

May 2015

ABSTRACT

Carbon Isotope Variations Associated with a Middle Ordovician Karstic Unconformity

By

Patricia Williams

Dr. Ganqing Jiang, Examination Committee Chair
Associate Professor of Geology University of
Nevada, Las Vegas

Large negative carbon isotope ($\delta^{13}C$) excursions have been documented from late Neoproterozoic-Paleozoic successions. These $\delta^{13}C$ excursions have been widely used for regional and global stratigraphic correlation, particularly in strata with limited paleontological and radiometric age controls. Recent studies, however, argued that some negative $\delta^{13}C$ excursions from stratigraphic record may have been resulted from meteoric/burial diagenesis, which commonly shifts both carbon and oxygen isotopes toward lower values. Testing the diagenetic origin of $\delta^{13}C$ excursions in stratigraphic successions without independent stratigraphic framework has been difficult because it evolves into circular arguments about stratigraphic completeness vs. diagenetic imprints. To address this issue, carbon and oxygen isotope analyses was conducted on the biostratigraphically controlled Middle Ordovician Antelope Valley Limestone Formation in the Arrow Canyon Range, Nevada, USA to document (1) the C-O isotope patterns of meter-scale cycles leading up to a well-known karstic unconformity and (2) isotope variability among carbonate lithologies and facies. The data are then compared with coeval isotope records regionally and globally to identify the maximum and minimum degree of isotope variations associated with meteoric/burial diageneses below a karstic

unconformity. The results may have implications for interpreting the origin of some negative $\delta^{13}C$ excursions, particularly those in the late Neoproterozoic.

ACKNOWLEDGEMENTS

Foremost, I would like to express my deepest gratitude to my advisor, Dr. Ganqing Jiang, you have been a great mentor to me and the advice you have given me on both my research and career path are priceless. Additionally, I would like to thank you for your patience with this project, spending countless hours correcting my writing, and financially supporting my research.

I would like to thank Dr. Terry Spell, Dr. Minghua Ren, and Dr. Brian Hedlund for serving on my committee and providing insightful comments and questions during my proposal defense and my final defense.

Additionally, I would like to thank the Graduate & Professional Student Association (GPSA) for providing a research grant to assist with funding of this project.

A special thanks to my family and friends, whom were always encouraging and offered their best wishes on days when I need support.

TABLE OF CONTENTS

LIST OF TABLES

LIST OF FIGURES

CHAPTER 1

INTRODUCTION

Carbon isotope values of marine carbonates ($\delta^{13}C_{carb}$) presumably record the isotope signature of seawater. In the modern ocean, the primary seawater $\delta^{13}C$ signature is close to 0‰. Because the ocean is well mixed and has a large dissolved inorganic carbon (DIC) reservoir (~3.8 x 10^{19} g carbon), any major departure in $\delta^{13}C_{carb}$ (exceeding 2‰ differences) from the average seawater signature require substantial changes in the global carbon cycle and oceanography. Large $\delta^{13}C_{carb}$ excursions from marine carbonate rocks are thus considered to be recording major paleoceanographic events and can be used for global stratigraphic correlation (e.g., Knoll et al., 1986; Brasier et al., 1994; Kaufman and Knoll, 1995; Saltzman et al., 1998; 2005; Halverson et al., 2005). However, because carbonate rocks and their associated isotope signatures can be modified by meteoric and burial diagenesis, to what degree the $\delta^{13}C_{carb}$ values from ancient rocks record seawater signature has been debated (e.g., Swart , 2008; Derry, 2010; Knauth and Kennedy, 2009; Swart and Kennedy, 2012; Oehlert and Swart, 2014).

The primary vs. secondary origin of $\delta^{13}C_{carb}$ excursions in late Neoproterozoic successions is a typical example of debate. Numerous studies have documented large negative $\delta^{13}C$ shifts with a nadir down to ≤ -5‰ (Kaufman and Knoll, 1995; Hoffman et al., 1998; Jacobsen and Kaufman, 1999; Halverson et al., 2005; Fike et al., 2006; Jiang et al., 2007; Grotzinger et al., 2011). These negative $\delta^{13}C_{carb}$ anomalies are difficult to interpret using traditional carbon cycle models because their minimum $\delta^{13}C_{carb}$ values are even lower than the average $\delta^{13}C_{carb}$ values of crustal rocks (≈ –5‰) and atmospheric CO_2 (≈ –6‰). Two interpretations have dominated in the last three decades.

In one interpretation, $\delta^{13}C_{carb}$ values obtained from Neoproterozoic carbonate-rich successions record a primary seawater signature because carbon is a major elemental component in carbonates, but a minor component in diagenetic fluids (e.g., Knoll et al., 1986; Kaufman et al., 1991; Kaufman and Knoll, 1995; Halverson et al., 2005; Jacobsen et al., 1999; Grotzinger et al., 2011). Under this assumption, $\delta^{13}C_{carb}$ anomalies can be a very useful chemostratigraphic tool for global stratigraphic correlation, particularly in strata with limited paleontological and radiometric age controls. They are also important evidence for substantial climate and oceanographic changes during the late Neoproterozoic, at the dawn of animal life (e.g., Hoffman et al., 1998; Halverson et al., 2005; Fike et al., 2006; Johnston et al., 2012).

The other interpretation emphasizes diagenetic overprints on Neoproterozic $\delta^{13}C_{carb}$ anomalies when carbonates interact with meteoric and formation fluids (e.g., Knauth and Kennedy, 2009; Swart and Kennedy, 2012). If carbonates were in contact with meteoric/formation fluids long enough and the fluid/rock ratios were high, rock-fluid interaction would significantly modify the isotope values of carbonate rocks. Therefore, using $\delta^{13}C$ anomalies for stratigraphic correlation and paleoceanographic interpretation would be problematic, particularly in strata with uncertain age constrains (e.g., Melezhik et al., 2001; Swart, 2008; Knauth and Kennedy, 2009; Derry, 2010; Swart and Kennedy, 2012; Oehlert and Swart, 2014).

Evaluating the diagenetic overprint on Neoproterozoic $\delta^{13}C_{carb}$ anomalies is difficult because of the inability to establish an independent chronostratigraphic framework in which $\delta^{13}C_{carb}$ values of coeval units can be confidently compared. This is

largely due to the lack of reliable paleontological data and radiometric ages in most Precambrian successions.

In a recent study, Knauth and Kennedy (2009) compiled the $\delta^{18}O$ and $\delta^{13}C_{carb}$ values of Neoproterozoic–Phanerozoic carbonates and found apparent co-varying $\delta^{13}C$–$\delta^{18}O$ trend. They interpreted that $\delta^{13}C_{carb}$ values falling on the co-varying $\delta^{13}C$–$\delta^{18}O$ trend and those $\delta^{13}C_{carb}$ scatters with more negative $\delta^{18}O$ values, were most likely formed during carbonate lithification and subsequent diagenetic alterations. Based on this, they concluded that the appearance of large negative $\delta^{13}C_{carb}$ anomalies in the late Neoproterozoic was possibly due to colonization of primitive land plants for the first time in Earth history. Other studies also demonstrated that the co-varying $\delta^{13}C$–$\delta^{18}O$ trend from carbonate rocks is an indicator of diagenetic alteration (e.g., Kaufman and Knoll, 1995; Derry, 2010). In contrast, an earlier study (Allan and Matthews, 1982) indicated that $\delta^{13}C$–$\delta^{18}O$ patterns vary along meteorically influenced surfaces. These uncertainties compel for more case studies across well-known karstic unconformities to better understand the isotope patterns associated with meteoric (and subsequent burial) diagenesis during sea-level fall events.

In this study, there will be an integrated sequence and chemostratigraphic study along the karstic unconformity below the Eureka Quartzite in the Mid-Late Ordovician section of the southern Great Basin (Figs. 1 and 2). By measuring carbon and oxygen isotopes of cyclic carbonate rocks below the Eureka Quartzite, this research will focus on (1) the temporal $\delta^{13}C$ –$\delta^{18}O$ pattern across a stratigraphic interval leading up to a karstic unconformity, (2) the $\delta^{13}C$ -$\delta^{18}O$ change within meter-scale carbonate cycles, and (3) the $\delta^{13}C_{carb}$ -$\delta^{18}O$ variations among different carbonate lithologies and facies. The overall

negative $\delta^{13}C_{carb}$ values and diagenetic $\delta^{13}C$ -$\delta^{18}O$ patterns below a karstic unconformity provide a case study for the diagenetic overprints on carbon and oxygen isotopes and may lend insights for understanding the origin of late Neoproterozoic negative $\delta^{13}C_{carb}$ excursions.

CHAPTER 2

STRATIGRAPHY, SAMPLING, AND ANALYTICAL METHODS

The Eureka Quartzite, at the middle-late Ordovician transition, is the most prominent siliciclastic unit within a more than 5000-m-thick, carbonate-dominated Paleozoic succession in the Great Basin (Langenheim et al., 1962; Fig. 3). The base of the Eureka Quartzite is a well-known karstic unconformity that may have had meteoric fluid influence tens to more than a hundred meter below the unconformity (e.g., Cooper and Keller, 2001). It serves as an ideal stratigraphic interval to understand meteoric diagenetic influences on carbon and oxygen isotope values. Preliminary isotope analyses by Kosmidis (2009) indicated that negative $\delta^{13}C_{carb}$ values below the Eureka Quartzite are common, but $\delta^{13}C_{carb}$ –$\delta^{18}O$ patterns are quite variable among different sections.

This study focuses on a 184-m-thick interval below the Eureka Quartzite in the northern Arrow Canyon Range (ACR) (Fig. 2). Stratigraphically, the study interval covers the upper part of the Pognip Group Unit E (Ope) and the entire Unit F (Opf) (Langenheim et al., 1962) (Fig. 3). Langenheim (1962) divided the Pogonip into 6 units, Opa-Opf. The Ope unit (0–55.5 meters) is almost entirely limestone with fossil sponges, brachiopods, echinoderms, trilobites, gastropods, and oncoids distributed throughout (Langenheim et al., 1962). The Opf unit (55.5–184 meters) has a gradational contact with Ope at the base, and unconformably underlies the Eureka quartzite. The lower part of Opf is limestone and the upper part, near the quartzite, is dolomite (Langenheim et al., 1962). This unit has fossil gastropods, bivalves, brachiopods, *Receptaculites* sp., and oncoids, which distinguishes from the Ope. *Receptaculites* sp. may correlate strata between Arrow Canyon and Ibex Hills (Langenheim et al., 1962; Stricker and Carozzi,

1973). The Opf of Langenheim (1962) in the Arrow Canyon Range is roughly correlatable with the Pogonip unit 9 in the Nopah Range (Cooper and Keller, 2001).

The age of Ope and Opf has not been precisely determined in this region, but according to available biostratigraphy, these units should be of late White Rockian or late Darriwilian-earliest Sandbian (Saltzman et al., 2005a, 2005b), near the Middle-Late Ordovician transition (Fig. 3).The Eureka Quartzite (EQ) has an estimated age of late Chatfieldian through late Edenian (Druschke et al., 2009). Existing carbon isotope studies from a few global successions show near zero or slightly negative (>-2‰) $\delta^{13}C_{carb}$ values across this time interval, but no significant negative $\delta^{13}C$ excursion has been documented (Fig. 4; Saltzman et al., 2005a, 2005b; Ainsaar et al., 2010; Munnecke et al., 2010; Albanesi et al., 2013). Recently negative $\delta^{13}C_{carb}$ values down to -5‰ are reported from strata below the Eureka Quartzite in central Nevada (Kosmidis, 2009; Edwards and Saltzman, 2014).

The karstic unconformity below the Eureka Quartzite in the region represents a prominent subaerial exposure/erosional surface (e.g., Cooper and Keller, 2001). The $\delta^{13}C_{carb}$ values below the Eureka Quartzite, if they have been altered by meteoric diagenesis, are expected to cover different stratigraphic thickness depending on the permeability of ancient carbonate facies and fluid penetration. The $\delta^{13}C_{carb}$–$\delta^{18}O$ patterns may vary, depending on the depth of the paleo-water table, intensiveness of water-rock interaction, and surface soil formation (Fig. 5; Allan and Matthews, 1982). Isotope values may vary among carbonate components such as micritic matrix, bioclasts and other particles including oncoids and ooids due to their differential resistance to diagenetic modification. Burial diagenetic fractures, cements, and structurally formed

veins would have distinguishable $\delta^{13}C_{carb}$ and $\delta^{18}O$ values. In addition, meter-scale cycles may show isotope variations, but the range of C-O isotope variations in individual cycles may be smaller than the isotope variations immediately below the karstic unconformity. Temporally, $\delta^{13}C_{carb}$ values should be most negative close to the unconformity and gradually change to the middle Ordovician background values away from the unconformity.

To test these hypotheses, samples were collected within a cyclo-stratigraphic framework to document the general $\delta^{13}C_{carb}$ -$\delta^{18}O$ pattern of Ope and Opf units, leading up to the base of the Eureka Quartzite. Detailed samples were collected temporally across two meter-scale cycles to test the amount of $\delta^{13}C_{carb}$ -$\delta^{18}O$ variations within individual cycles. In addition, large rock slabs that contain bioclasts, oncoids, and/or later diagenetic cements or veins have been collected to test the isotope variations among carbonate components. A total of 188 samples were analyzed for $\delta^{13}C_{carb}$ and $\delta^{18}O$ values.

Hand samples were cut perpendicular to bedding in the University of Nevada Las Vegas Rock Preparatory Laboratory. Sixteen of those samples were sent to Quality Thin Sections to be polished and thin sectioned for petrographic study of diagenetic sequence.

For isotope analyses, carbonate powders (10–15 mg) were drilled from cleaned slabs. About 50–200 μg of sample powders were reacted with orthophosphorous acid for ten minutes at 70 °C in the Kiel IV Carbonate Device to generate purified CO_2, which was transferred to the dual-inlet Finnigan Delta V Plus Mass Spectrometer for carbon and oxygen isotope analysis. Analytical reproducibility was better than 0.1‰ for both $\delta^{13}C_{carb}$ and $\delta^{18}O$ values, as monitored by NBS-19 and an internal standard. The isotope analyses

and sample preparation were conducted at the Las Vegas Isotope Science laboratory (LVIS) at University of Nevada-Las Vegas.

CHAPTER 3

FACIES AND FACIES ASSOCIATIONS

Ten lithofacies are identified from the 184-m-thick section of the Antelope Valley Limestone Formation. These include (1) Thick-massive oncolitic-oolitic-bioclastic grainstone/packstone, (2) Oncolitic-bioclastic packstone with mudstone/lime mudstone lenses/drapes, (3) Bioclastic-oncolitic wackestone with mudstone/lime mudstone lenses, (4) Interbedded mudstone/lime mudstone with packstone interbeds, (5) Bioclastic lime mudstone/mudstone, (6) Oolitic-peloidal grainstone, (7) Intraclastic-bioclastic grainstone-packstone, (8) Bioclastic-peloidal wackestone, (9) Dolomitic lime mudstone with dissolution cavities, and (10) Microcrystalline dolostone. Their major features including constituents, bedding, and sedimentary structures are summarized in Table 1. The depositional model of these facies is delineated in Fig. 6 and some of their field/petrographic features are provided in Figures 7-10.

These facies are grouped into four facies associations according to their depositional environments including oncolitic-oolitic sand shoal, shallow lagoon, shallow subtidal, and tidal flat facies associations (Fig. 6A). The depositional environments of the measured section (Fig. 7) temporally changed from a rimmed carbonate shelf with a shoal complex at the shelf margin (0-82 m) to a shallow lagoon environment (83-113 m), and to open shelf peritidal (shallow subtidal and tidal flat) environments in the upper part (114-176 m). The measured section records an overall shallowing-upward sequence with facies prograding toward the west. In addition to the unconformity at the base of the Eureka Quartzite, three stratigraphic discontinuities characterized by abrupt facies change

are identified at 113 m, 137 m, and 172 m; their regional extension and significance requires further investigation (Fig. 7).

3.1 Oncolitic-oolitic sand shoal facies association

The sand shoal facies association occurs in the lower part of the measured section (0–82 m). It consists of three lithofacies (Table 1): thick-massive oncolitic-oolitic-bioclastic grainstone/packstone (Facies 1), oncolitic-bioclastic packstone with mudstone/lime mudstone lenses/drapes (Facies 2), and bioclastic-oncolitic wackestone with mudstone/lime mudstone lenses (Facies 3). The grainstones-packstones are commonly 0.5–2 m thick. Oncoids vary from 5%–50% abundance and their sizes range from 0.5 cm to 2 cm (e.g., Figs. 8A). The remaining particles are ooids and bioclasts (Fig. 10A and B), which vary in abundance both laterally and vertically. *Receptaculites* sp. is found in varying abundance in this facies, but mostly in the upper part after 72 meters of the section. Some grainstone beds have erosional bases with 1–2 cm minor relief and occasionally, higher erosional relief (up to 5–10 cm) and cross bedding are observed.

In outcrop, oncolitic-bioclastic packstone with mudstone/lime mudstone lenses/drapes (Facies 2) looks similar to Facies 1 and the contact between these two facies are transitional. The most characteristic feature of this facies is the presence of thin (< 3 cm) lime mudstone/mudstone lenses and drapes (e.g., Fig. 8B). The lime mudstone/mudstone is laterally discontinuous and pinches out within decimeter distance possibly due to compaction. Bioclastic-oncolitic wackestone with mudstone/lime mudstone lenses (Facies 3) forms thin (< 10 cm) to medium (10–30 cm) beds with undulated bedding planes. In comparison with Facies 2, this facies is proportionally more

enriched in mudstone/lime mudstone and contains laterally variable but continuous mudstone/lime mudstone beds (< 5 cm). Oncoids and bioclasts are unevenly distributed in this facies.

The thick-massive grainstones/packstones (Facies 1) are interpreted to have formed in high-energy environments above fair-weather wave base, as evidenced by the presence of erosional bases in some grainstone beds and occurrence of cross bedding. The thick beds and persistent occurrence of this facies suggest deposition from a high-energy oncolitic-oolitic sand_shoal complex close to the shelf margin (Fig. 6A). This is consistent with previous interpretations based on the regional distribution of oncolites (Gunn, 1998). Oncolitic-bioclastic packstone with mudstone/lime mudstone lenses/drapes (Facies 2) and bioclastic-oncolitic wackestone with mudstone/lime mudstone lenses (Facies 3) are interpreted as deposition from partially protected, distal tidal flat environments. The presence of thin (< 5 cm) lime mudstone/mudstone lenses may indicate progradational migration of back-barrier lagoonal deposits towards the shelf margin shoal complex (Fig. 6A).

3.2 Shallow lagoon facies association

The shallow lagoon facies association consists of oncolitic-bioclastic packstone with mudstone/lime mudstone lenses/drapes (Facies 2), bioclastic wackestone with mudstone/lime mudstone lenses (Facies 3), interbedded mudstone/lime mudstone with packstone interbeds (Facies 4) and bioclastic lime mudstone/mudstone (Facies 5). In comparison with the sand shoal facies association, this facies association is characterized by the decrease of grainstone and increase of lime mudstone and mudstone facies.

The packstone and wackestone facies (Facies 2 and 3; Table 1) form thin (< 10 cm) to medium (10-30 cm) beds with laterally discontinuous lime mudstone/mudstone lenses or thin (< 5 cm) layers (Fig. 8C). Differential compaction leads to undulated bedding planes. Bioclasts are the main particle type, including well-preserved, centimeter-scale gastropods and *Receptaculites* (Fig. 9A and B). Oncoids are also present (Fig. 9B) but much less abundant than those in the sand shoal facies. The mudstone and lime mudstone facies (Facies 4 and 5; Table 1) occur as thin (< 10 cm) beds, with variable wackestone/packstone layers/lenses (Fig. 8D). Differential compaction resulted in lateral thickness change, forming mottled texture (Fig. 9C and D). Well-preserved *Receptaculites* and gastropods are unevenly distributed and often penetrate through the lithological boundaries (Fig. 9C and D). Some crawling traces were found along the bedding planes of mudstone/lime mudstone, but they are often distorted or broken due to compaction.

The wackestone, lime mudstone and mudstone facies (Facies 3, 4, and 5) are interpreted as subtidal lagoon deposits likely formed below fair-weather wave base. Presence of packstone interbeds and detrital biolasts/oncoids in wackestone-limestone-mudstone facies suggests sediment transportation by storm or high tidal waves. The thick packstone facies (Facies 2) was more likely formed in shallow-subtidal environments of the shallow lagoon, close to or above fair-weather wave base. The lagoon may have been restricted from open ocean by the oncolitic-oolitic sand shoal complex at the shelf margin (Fig. 6A), but it may have remained shallow, as evidenced by the close association with packstone and grainstone facies.

3.3 Shallow subtidal facies association

The shallow subtidal facies association consists of oolitic-peloidal grainstone and intraclastic-bioclastic grainstone-packstone (Facies 6 and 7; Table 1). Oolitic-peloidal grainstones form 0.3–1.0 m thick beds that commonly have minor erosional bases at the bottom. Small-scale (<20 cm) cross beddings are occasionally observed. Intraclastic-bioclastic grainstones (e.g., Fig. 10D) form medium (10–30 cm) to thick (>30 cm) beds and have thin (<5 cm), laterally discontinuous shaly (muddy) partings along bedding planes (e.g., Fig. 8E). Intraclasts vary in size from 5 mm to 5 cm and are unevenly distributed; most of them have angular shapes (Fig. 8E) and composition of mudstone/lime mudstone.

The grainstone facies defined here refers to the facies appearing in the upper part of the measured section (113–184 m; Fig. 7). They are interpreted as deposits from shallow subtidal environments above fair-weather wave base in the proximal side of the shelf lagoon or in open shelf after the lagoon has been filled up. The presence of unsorted and angular intraclasts suggests intraclast formation in tidal flats and transportation into subtidal environments by storm waves or high tides.

3.4 Tidal flat facies association

The tidal flat facies association consists of mixed dolomite-limestones including bioclastic-peloidal wackestone, dolomitic lime mudstone with dissolution cavities, and microcrystalline dolostone (Facies 8, 9, and 10 in Table 1). Thin (<10 cm) intraclastic-bioclastic packstone (Facies 6 in Table 1) layers are also present. Bioclastic-peloidal wackestone (Facies 8) form thin (<10 cm) to medium (10–30 cm) beds with ≤ 5-cm-thick

mudstone interbeds/lenses (e.g., Fig. 10C). A significant amount (up to 10%) of quartz and feldspar are present in both wackestone and mudstone interbeds (Fig. 10C). Bioclasts are unevenly distributed within lime mudstone matrix. Occasionally microbial laminae and fenestral structures are observed. Dolomitic lime mudstone (Facies 9) appears in thin (<10 cm) beds and less commonly, medium (10–30 cm) beds, separated by yellowish-reddish mudstone (e.g., Fig. 8F). Bioclasts are present but laterally variable in abundance and sizes. Dissolution cavities (e.g., Fig. 10E), vugs and "popcorn" quartz are found in some intervals. Microcrystalline dolostone (e.g., Fig. 10F) form thick (>30 cm) amalgamated beds containing vugs and cavities filled with white calcite crystals. Thin (< 3 cm) mudstone lenses/layers are also found in some intervals of the dolostone facies.

The wackestone, dolostone and dolomitic lime mudstone facies are interpreted as deposition from intertidal to supratidal environments as evidenced by shallow-water features including microbial laminae, fenestral structures, dissolution cavities, vugs, and siliciclastic components (quartz and feldspar). Thin packstone layers may have deposited during high tides or storm events.

CHAPTER 4

METER-SCALE CARBONATE CYCLES

Three types of meter-scale cycles are identified from the measured section of the Antelope Valley Formation (Figs. 6B and 7). The sand shoal cycles have oncolitic-oolitic-bioclastic grainstone facies (Facies 1) at the lower part and packstones/wackestone with mudstone/lime mudstone lenses (Facies 2 and 3) at the top. The change from massive grainstone to packstone/wackestone facies records a shallowing-up trend from subtidal to intertidal or progradation of lagoonal facies on the top of sand shoal facies during sea-level fall. Shallow lagoonal cycles consist of wackestone- and mudstone/lime mudstone-dominated facies (Facies 3, 4 and 5) in the lower part and packstone/grainstone (Facies 2) at the top, recording shallowing-upward trend from deep-subtidal (below fair-weather wave base) to shallow subtidal (above fair-weather wave base) environments during sea-level fall. Peritidal cycles defined here refer to those from the upper part (113–184 m) of the measured section (Fig. 7). They consist of packstone/grainstone facies (Facies 6 and 7) at the base and wackestone/lime mudstone/dolostone facies (Facies 8, 9, and 10) in the upper part, recording shallowing-upward trends from shallow subtidal to intertidal/supratidal environments. Exposure features are found only at the top of some peritidal cycles, but not in shallow lagoon and sand shoal cycles.

The *Receptaculites* sp. is present in the upper part of the sand shoal facies but is most abundant in the lagoon facies (82–113 m), suggesting their preference of living in low-energy environments. The disappearance of *Receptaculites* sp. in the upper part of the measured section (113–184 m) also suggests that shallow-water environments with periodic exposure were not their environmental niche.

CHAPTER 5

ISOTOPE RESULTS

In general, $\delta^{13}C$ values from the upper Antelope Valley Limestone Formation (Ope and Opf) are all negative (Fig. 7). From 0 m to 110 m, $\delta^{13}C$ values fall between –0.5‰ and –2.5‰, with the majority of data points in the range of –1.0‰ ~ –2.0‰. Large $\delta^{13}C$ variations of –5.5‰ to –1.8‰ (average = –3.0‰) are found from 110 to 170 m, followed by a slightly positive shift to –1.7‰ within the 14-m-thick dolostones immediately below the Eureka Quartzite (Fig. 7). The only positive $\delta^{13}C$ value of 0.06‰ is found at 178 m (8 m below the Eureka Quartzite), but because this is a single data point, its geochemical meaning needs further tests by sampling adjacent strata at much higher resolution.

The majority of $\delta^{18}O$ values from the measured sections fall between –6‰ and –8‰ (Fig. 7). Higher $\delta^{18}O$ values from –4.4‰ to –0.6‰ are found in the dolostone interval (172–186 m) below the Eureka Quartzite, exhibiting a "positive" shift (Fig. 7). However, because the reported isotope results did not correct the potential calcite-dolomite isotope fractionation (e.g., Rosenbaum et al., 1986; Dickenson et al., 1980), such a "positive" shift may record the oxygen isotope changes during dolomitization.

There is no $\delta^{13}C$–$\delta^{18}O$ co-variation when all the samples are considered together, but the $\delta^{13}C$–$\delta^{18}O$ patterns seem to vary with sedimentary facies (Fig. 11). The peritidal facies from 114 m to 172 m have the most diverse $\delta^{13}C$ values (–1.8‰ to –5.5‰) and least variable $\delta^{18}O$ (–5.5‰ to -7.5‰), while shallow lagoon and sand shoal facies (0–113 m) have both narrow $\delta^{13}C$ (mostly –1‰ to –2‰) and $\delta^{18}O$ (–6‰ to –8‰). In contrast,

the peritidal dolostone facies immediately below the Eureka Quartzite show an obvious $\delta^{13}C$–$\delta^{18}O$ co-variation (Fig. 11).

Except for the dolostones below the Eureka Quartzite, there are no obvious lithology-dependent isotope variations (Fig. 12). Packstones and grainstones do have a slightly wider range of $\delta^{13}C$ (–5.5‰ to –0.5‰) and $\delta^{18}O$ (–6.0‰ to –8.5‰) than those of the lime mudstone ($\delta^{13}C$: –5.2‰ to –2.7‰; $\delta^{18}O$: –6.0‰ to –7.6‰) and wackestone ($\delta^{13}C$: –4.7‰ to –1.7‰; $\delta^{18}O$: –5.5‰ to –8.0‰), but the isotope differences between adjacent lithologies are almost indistinguishable. In addition, no significant or systematic $\delta^{13}C$ or $\delta^{18}O$ changes have been found among lithologies of meter-scale cycles (e.g., Fig. 13), although the current sample resolution is insufficient to draw a general conclusion about cycle-related isotope variations.

CHAPTER 6

DISCUSSION

6.1 The negative $\delta^{13}C$ 'excursion' below the unconformity: Not an oceanographic signature

The $\delta^{13}C$ profile of the Antelope Valley Limestone Formation in Arrow Canyon Range displays a negative 'excursion' with minimum $\delta^{13}C$ values down to $\leq$ –5‰ below the basal unconformity of the Eureka Quartzite (Fig. 7). Negative $\delta^{13}C$ shifts down to –5‰ have been also documented from other sections in the Great Basin (Fig. 14), including the Shingle Pass and Ibex Hills sections (Edwards and Saltzman, 2014) and the Pahranagat Range, Hot Creek, and Lone Mountain sections (Kosmidis, 2009). However, in other global successions, time-equivalent strata have much less prominent negative $\delta^{13}C$ values. For example, Middle-Late Ordovician (Darriwilian–Sandbian; ca. 467–453 Ma) strata in Baltoscandia have $\delta^{13}C$ values mostly positive or close to 0‰ (Fig. 4; Ainsaar et al., 2010). The Middle-Late Ordovician strata from the Borenshult Drillcore in Sweden do not have negative $\delta^{13}C$ values or a negative $\delta^{13}C$ shift during Darriwilian (Bergström et al., 2012; Calner et al., 2014). The Middle-Late Ordovician strata in Western Newfoundland and sections from Precordillera of Argentina do not have $\delta^{13}C$ values lower than –2‰ (Thompson and Kah, 2011; Albanesi et al., 2013). Even in the Great Basin, Darriwilian strata in some sections such as the Monitor-Antelope Range section do not have negative $\delta^{13}C$ values lower than –2.5‰ (Fig. 4; Kump et al., 1999; Saltzman et al., 2005).

The $\delta^{13}C$ heterogeneity of Darriwilian strata in the Great Basin and across the globe (Figs. 4 and 14) suggests that the negative $\delta^{13}C$ 'excursion' below the Eureka Quartzite

does not record a paleoceanographic signature. Instead, it may record a localized signature of a restricted basin or a diagenetic feature (e.g., Panchuk et al., 2006; Edward and Saltzman, 2014). Because local $\delta^{13}C$ variations up to –5‰ isotopic departure from open-ocean signature have been observed in modern lagoonal environments (e.g., Patterson and Walter, 1994; Swart et al., 2009), it can be argued that the negative $\delta^{13}C$ 'excursion' from the Arrow Canyon Range section was formed in a restricted environment. Facies analysis of the measured section (Figs. 6 and 7) and previous stratigraphic correlation (e.g., Gunn, 1998) suggest that the 30-m-thick stratigraphic interval from 82 m to 113 m was most likely deposited from lagoonal environments behind a shelf-margin shoal complex, but $\delta^{13}C$ values of that interval do not show significant changes in $\delta^{13}C$ (Fig. 7). In addition, the depth of the negative $\delta^{13}C$ 'excursion' below the Eureka Quartzite is highly variable (Fig. 14), from immediately below the Eureka Quartzite in the Lone Mountain section, to 25 m below the Eureka Quartzite in the Hot Creek Range, and to 50–150 m below the Eureka Quartzite in Shingle Pass, Ibex Hills, and Arrow Canyon Range sections. It seems that the negative $\delta^{13}C$ 'excursion' is more related to the stratigraphic position relative to the basal Eureka unconformity, rather than a particular facies deposited from restricted environments. The $\delta^{13}C$–$\delta^{18}O$ patterns differ among the Great Basin sections (Fig. 15), with varying amount of data points falling into the lithification trend and burial diagenetic region of Knauth and Kennedy (2009). All these features indicate that the negative $\delta^{13}C$ shift of the uppermost Antelope Valley Limestone Formation was formed through various diagenetic alterations below an unconformity.

6.2 A diagenetic interpretation for the negative $\delta^{13}C$ 'excursion'

The variable $\delta^{13}C$ profiles (Fig. 14) and $\delta^{13}C$–$\delta^{18}O$ patterns (Fig. 15) below the Eureka Quartzite suggest meteoric diagenetic alteration of isotope values with the development of vadose, freshwater phreatic, and mixing zones during the sea-level fall and exposure, similar to those documented from the Latest Devonian (Myrow et al., 2013) and Pliocene–Pleistocene (Swart and Kennedy, 2012) strata. In all those cases, absolute $\delta^{13}C$ and $\delta^{18}O$ values and their alteration depth below an unconformity may vary spatially, but a negative $\delta^{13}C$ shift is observed in most sections. The $\delta^{13}C$–$\delta^{18}O$ patterns and the depth of alterations may record variations of the paleo-water table and intensity of fluid-rock interactions (e.g., Allan and Matthews, 1982).

The co-variation of $\delta^{13}C$ and $\delta^{18}O$ from the uppermost 20 m of the measured section (Fig. 11) is similar to the $\delta^{13}C$–$\delta^{18}O$ pattern of the mixing zone of Allan and Matthews (1982) (Fig. 5D) and the burial diagenetic pattern of Derry (2010), but the close proximity to the base of the Eureka Quartzite suggests that this interval most likely records the isotope alterations of the paleo-vadose zone. The large $\delta^{13}C$ variations but limited $\delta^{18}O$ change from 114-170 m (Fig. 11) is similar to the general meteoric diagenetic pattern of Allan and Matthews (1982) (Fig. 5B) or the pattern close to the water table (Fig. 5C). Since the negative $\delta^{13}C$ 'excursion' mainly occurs in this interval, it suggests that the magnitude of $\delta^{13}C$ variations may have been controlled by the paleo-water table. Since the depth of the paleo-water table may be controlled by the paleobathymetry or paleo-topography of the carbonate platform and lithologies (e.g., clay-rich layers) that can potentially serve as an aquifuge, the most intensively altered

$\delta^{13}C$ interval could be meters to tens of meters below the unconformity. In this case, using the negative $\delta^{13}C$ shift to infer the ancient karstic uniformity requires additional physical stratigraphic evidence (cf., Cooper et al., 2001; Swart and Kennedy, 2012; Myrow et al., 2013).

The overall negative $\delta^{13}C$ and $\delta^{18}O$ values of the Antelope Valley Limestone Formation in Arrow canyon Range suggest overlapped diagenetic alterations. This is consistent with the presence of calcite twins in thin sections and oxygen isotope values mostly below –6‰ in the majority of the Great Basin sections (Fig. 15). However, the oxygen isotopes temporally vary in the same section and among sections at magnitudes of 4–10‰ (Fig. 15), using the $\delta^{13}C$–$\delta^{18}O$ crossplots of measured sections to screen out diagenetic samples, as many have used in the literature, is impractical and sometimes, misleading. The similar range of $\delta^{13}C$ and $\delta^{18}O$ variations in lime mudstones and grainstones (Fig. 12) also implies that the traditional practice of using fine-grained carbonates for isotope analyses unnecessarily improves the $\delta^{13}C$ record of stratigraphic successions. Instead, micro-recrystallization of lime mud (e.g., Fig. 10E and F) during diagenesis may lead to isotope alterations even more severe than in grainstones and packstones.

6.3 Implication for late Neoproterozoic negative $\delta^{13}C$ excursions

The presence of negative $\delta^{13}C$ shift with a nadir of –5.5‰ below the basal Eureka Quartzite adds to the notion that some of the prominent late Neoproterozoic $\delta^{13}C$ excursions may be related to meteoric diagenesis associated with sea-level fall and exposure (e.g., Knauth and Kennedy, 2009; Derry, 2010; Swart and Kennedy, 2012; Myrow et al., 2013; Oehlert and Swart, 2014). Although it is expected that meteoric

diagenesis is localized or regional and $\delta^{13}C$ anomalies of diagenetic origin should be less consistent and spatially variable as seen in the examples of Middle Ordovician (Fig. 14), Latest Devonian (Myrow et al., 2013) and Pliocene–Pleistocene (Swart and Kennedy, 2012), some of the Ediacaran $\delta^{13}C$ excursions do show large spatial variations. Examples include the Shuram-equivalent $\delta^{13}C$ excursion in South China (Doushantuo Member III, Jiang et al., 2007, 2008, 2011; Zhu et al., 2007, 2013; Lu et al, 2013) and in northern India (Krol B; Jiang et al., 2002; Kaufman et al., 2006) where (1) the thickness of strata that host the negative $\delta^{13}C$ excursion varies from a few meters to tens of meters; (2) $\delta^{13}C$ values vary from –5‰ to –12‰; and (3) $\delta^{13}C$–$\delta^{18}O$ patterns change from a positive co-variance in some sections to large $\delta^{13}C$ but small $\delta^{18}O$ variations in other sections. These features are very similar to the $\delta^{13}C$–$\delta^{18}O$ patterns presented in this study and in other examples (e.g., Swart and Kennedy, 2012; Myrow et al., 2013). The variable diagenetic $\delta^{13}C$–$\delta^{18}O$ patterns below unconformities (e.g., Fig. 11) cast doubt on the common practice of using the co-variation of $\delta^{13}C$ and $\delta^{18}O$ to screen out diagenetic samples (e.g., Kaufman and Knoll, 1995).

The Ediacaran Shuram $\delta^{13}C$ excursion in Oman was documented from a transgressive succession (e.g., Fike et al., 2006; Grotzinger et al., 2011). However, the negative $\delta^{13}C$ excursion from the upper Doushantuo Formation in South China has been variously ascribed as a transgressive sequence (e.g., Zhu et al., 2013) or regressive sequence (e.g., Jiang et al., 2007; Wang et al., 2014). The Shuram-equivalent $\delta^{13}C$ excursion in northern India (Jiang et al., 2002; Kaufman et al., 2006) mainly occurs in the regressive part of a sequence (Krol B). Apparently the relationships between late

Neoproterozoic $\delta^{13}C$ excursions and stratigraphic unconformities remain critical to interpret the origin of some unusually negative $\delta^{13}C$ excursions.

CHAPTER 7

CONCLUSION

Sedimentological and isotope analyses of the Middle Ordovician carbonate-rich strata in the Arrow Canyon Range of southern Nevada, USA, reveal a negative $\delta^{13}C$ 'excursion' with a nadir down to –5‰ below a karstic unconformity at the base of the Middle-Late Ordovician Eureka Quartzite. Negative $\delta^{13}C$ values do not co-vary with $\delta^{18}O$ in general and seem to be lithologically independent. Similar negative $\delta^{13}C$ values have been documented from other correlative sections in the Great Basin but occur at variable depths below the basal Eureka Quartzite. The spatially variable $\delta^{13}C$ profiles and $\delta^{13}C$–$\delta^{18}O$ patterns suggest meteoric diagenetic origin for the isotope anomaly that may have been controlled by the depth of the paleo-water table. While diagenetic $\delta^{13}C$ anomalies could potentially be used for stratigraphic correlation because they are associated with sea-level fall and exposure, the most intensive $\delta^{13}C$ alteration may happen at the stratigraphic interval close to the water table. The water table could be up to tens-hundreds of meters below the unconformity, depending on the paleobathymetry/topography of the carbonate platform and lithologies that can serve as an aquifuge. Therefore, using negative $\delta^{13}C$ anomalies to track ancient sea-level fall/exposure requires integrated sequence stratigraphic and isotope analyses.

The presence of negative $\delta^{13}C$ anomalies below karstic unconformities in Ordovician strata and in many other stratigraphic intervals such as the Latest Devonian and Pliocene–Pleistocene strata add to the notion that some of the late Neoproterozoic negative $\delta^{13}C$ excursions may be of diagenetic origin. Typical examples may include the upper Doushantuo $\delta^{13}C$ excursion in South China and the Krol B $\delta^{13}C$ excursion in northern

India. In both cases 1Pc profiles show large spatial variations and variable IPC--0^{18}O patterns similar to those presented in this study.

Table 1. Summary of facies of the upper Antelope Valley Limestone Formation in Arrow Canyon Range.

Facies	Constituents	Bedding	Sedimentary Structures	Interpretation
Thick-massive oncolitic-oolitic-bioclastic grainstone/packstone (1)	Spherical-oval oncoids of 3-10 mm in size. Oncoids constitute 5-50% of the grains. Ooids are 0.2-2 mm in size and vary in contents from 10-20%; occasionally up to 80%, forming oolite layers. Bioclasts are unevenly distributed, including brachiopod, gastropod, triolobite, and echinoderm fossil fragments. Occasional intraclasts consists of mudstone/lime mudstone.	Thick (30-100 cm) to massive (> 1 m) beds. Erosional surfaces at the base and in cases, internal erosional surfaces are observed.	Cross-bedding is occasionally observed.	High-energy shallow subtidal oncolitic-oolitic sand shoals
Oncolitic-bioclastic packstone with mudstone/lime mudstone lenses/drapes (2)	Oncoids (3-10 mm) and bioclasts are the dominated grains. Oncoids constitute 5-30%; the rest of the grains are mixed bioclasts and peloids. Occasionally ooids can be seen.	Thin (< 10 cm) to medium (10-30 cm) packstone beds with laterally discontinuous, thin (< 3 cm) lime mudstone-mudstone beds/lenses or drapes.	Mudstone drapes; firmground (hardened lime mudstone).	Moderate- to high-energy peritidal environments close to shoal complex or subtidal lagoon
Bioclastic-oncolitic wackestone with mudstone/lime mudstone lenses (3)	Spherical and in cases, asymmetric oncoids and bioclasts unevenly distributed in lime mud matrix.	Thin (< 10 cm) to medium (10-30 cm) wackestone beds with laterally discontinuous lime mudstone-mudstone. Undulated bedding planes.	Mudstone drapes, bioturbation.	Moderate- to low-energy peritidal close to shoal complex or subtidal lagoon
Interbedded mudstone/lime mudstone with packstone interbeds (4)	Bioclasts (brachiopod, gastropod, trilobites, and echinoderm fragments) unevenly distributed in mudstone matrix. Some well-preserved gastropods and *Receptaculites*.	Thin (< 10 cm) beds. Packstone beds are laterally variable and have undulated bedding planes due to compaction.	Bioturbation; minor erosional surfaces at the base of packstones.	Protected, low-energy subtidal lagoon with storm events (packstones).
Bioclastic lime mudstone/mudstone (5)	Bioclasts unevenly distributed in mudstone and lime mudstone matrix. Some well-preserved *Receptaculites*.	Thin (< 10 cm) undulated beds; some beds laterally pinches out within decimeter-meter distance	Bioturbation; occasional trace fossils.	Protected, low-energy subtidal lagoon environments
Oolitic-peloidal grainstone (6)	Ooids and peloids with minor bioclasts	Thick (30-100 cm) beds with erosional bases.	Occasional cross bedding.	High-energy shallow subtidal environments.

Intraclastic-bioclastic grainstone-packstone (7)	Mudstone/lime mudstone intraclasts; angular-subangular, 0.5-5 cm in size. Bioclasts unevenly distributed.	Medium (10-30 cm) and thick (> 30 cm) beds with thin shaley (muddy) partings	Undulated bedding; minor erosional bases below intraclastic grainstone beds	High-energy shallow subtidal environments.
Bioclastic-peloidal wackestone (8)	Bioclasts and peloids (and minor oncoids) unevenly distributed in lime mud matrix	Thin (< 10 cm) to medium (10-30 cm) beds with very thin (< 5 mm) mudstone interbeds.	Occasional fenestral structures and dissolution cavities.	Low-energy intertidal-supratidal environments.
Dolomitic lime mudstone with dissolution cavities (9)	Sparse fossil fragments	Thin (< 10 cm) to medium (10-30 cm) undulated beds	Bioturbation; dissolution cavities, vugs	Low-energy intertidal-supratidal environments.
Microcrystalline dolostone (10)	microcrystalline dolomites; occasional intraclasts	Thick (> 30 cm) amalgamated beds with muddy lenses	Voids and cavities filled with coarse calcite	Low energy intertidal-supratidal environments.

Table 2. Carbon and oxygen isotope results from the upper Antelope Valley Limestone Formation in the Arrow Canyon Range, southern Nevada, USA.

Table 2: Inorganic carbon isotope data from the Mid-Late Ordovician (ca. 468-460 Ma)									
Section 1: Arrow Canyon Range, Southern Nevada GPS Coordinates (36º43'34.75 N, 114º53'29.24 W)									
Stratigraphic unit	**Sample No.**	**Strat. Height**	**Lithology**	**Drilled Lithology**	**$\delta^{13}C$ (‰, VPDB)**	**$\delta^{18}O$(‰, VPDB)**	**Age**	**Depo. Environment**	**Langenheim et al. Subdivisions**
Antelope Valley Limestone	ACO-1.1	1.1	intraclastic packstone	packstone	-0.80	-7.53	Darriwilian	Sand Shoal Complex	Ope
Antelope Valley Limestone	ACO-2.1	2.1	intraclastic-bioclastic grainstone	grainstone	-0.72	-7.11	Darriwilian	Sand Shoal Complex	Ope
Antelope Valley Limestone	ACO-2.3	2.3	bioclastic grainstone-packstone w/ muddy interbeds (<5mm)	grainstone-packstone	-0.35	-6.59	Darriwilian	Sand Shoal Complex	Ope
Antelope Valley Limestone	ACO-3.2	3.2	bioclastic lime-mudstone w/ shaley parting (<2mm)	lime mudstone	-1.03	-8.38	Darriwilian	Sand Shoal Complex	Ope
Antelope Valley Limestone	ACO-4.3	4.3	packstone	packstone	-0.73	-7.46	Darriwilian	Sand Shoal Complex	Ope
Antelope Valley Limestone	ACO-5.2	5.2	packstone-wackestone	packstone-wackestone	-1.01	-7.58	Darriwilian	Sand Shoal Complex	Ope
Antelope Valley Limestone	ACO-6	6	bioclastic-oolitic grainstone	grainstone	-0.98	-7.44	Darriwilian	Sand Shoal Complex	Ope
Antelope Valley Limestone	ACO-7.1	7.1	bioclastic-intraclastic grainstone	grainstone	-0.71	-7.27	Darriwilian	Sand Shoal Complex	Ope

Antelope Valley Limestone	ACO-9.2	9.2	oncolitic-oolitic grainstone	grainstone	-1.35	-7.38	Darriwilian	Sand Shoal Complex	Ope
Antelope Valley Limestone	ACO-10	10	oolitic-bioclastic grainstone has birds eye lenticular voids, calcite vein (2mm thick), tan mud lenses	grainstone	-1.05	-7.24	Darriwilian	Sand Shoal Complex	Ope
Antelope Valley Limestone	ACO-11	11	oolitic grainstone	grainstone	-1.21	-7.08	Darriwilian	Sand Shoal Complex	Ope
Antelope Valley Limestone	ACO-12	12	bioclastic-oolitic packstone	packstone	-1.29	-7.58	Darriwilian	Sand Shoal Complex	Ope
Antelope Valley Limestone	ACO-13	13	bioclastic-oolitic grainstone	grainstone	-1.38	-7.74	Darriwilian	Sand Shoal Complex	Ope
Antelope Valley Limestone	ACO-14.2	14.2	packstone with mudstone lenses	packstone	-1.54	-7.32	Darriwilian	Sand Shoal Complex	Ope
Antelope Valley Limestone	ACO-15.1	15.1	packstone with mudstone lenses	packstone	-1.48	-7.21	Darriwilian	Sand Shoal Complex	Ope
Antelope Valley Limestone	ACO-16.2	16.2	bioclastic-grainstone w/ few mudstone intraclasts	grainstone	-1.23	-7.11	Darriwilian	Sand Shoal Complex	Ope
Antelope Valley Limestone	ACO-17.1	17.1	grainstone/packstone	grainstone/packstone	-1.49	-7.24	Darriwilian	Sand Shoal Complex	Ope
Antelope Valley Limestone	ACO-18	18	grainstone wavy surficial weathering pattern, coral frag.	grainstone	-1.86	-7.56	Darriwilian	Sand Shoal Complex	Ope
Antelope Valley Limestone	ACO-19	19	bioclastic packstone	packstone	-1.73	-7.28	Darriwilian	Sand Shoal Complex	Ope
Antelope Valley Limestone	ACO-20	20	bioclastic packstone	packstone	-1.51	-6.68	Darriwilian	Sand Shoal Complex	Ope
Antelope Valley Limestone	ACO-21	21	bioclastic packstone	packstone	-1.73	-7.76	Darriwilian	Sand Shoal Complex	Ope

Antelope Valley Limestone	ACO-22	22	oncolitic-bioclastic grainstone & mudstone (<5mm) interbeds. slightly less degree of light gray (slightly less recrystallized) as 2.1&2.3	grainstone	-1.55	-7.24	Darriwilian	Sand Shoal Complex	Ope
Antelope Valley Limestone	ACO-23.8	23.8	oncolitic-bioclastic packstone with thin grainstone (3-7cm) & mudstone (<5mm) interbeds. slightly less degree of light gray (slightly less recrystallized) as 2.1&2.4	packstone	-1.44	-7.26	Darriwilian	Sand Shoal Complex	Ope
Antelope Valley Limestone	ACO-24.9	24.9	bioclastic packstone-wackestone	packstone-wackestone	-1.55	-7.16	Darriwilian	Sand Shoal Complex	Ope
Antelope Valley Limestone	ACO-26.1	26.1	bioclastic wackestone, thin mud interbeds	wackestone	-2.13	-7.98	Darriwilian	Sand Shoal Complex	Ope
Antelope Valley Limestone	ACO-27	27	bioclastic wackstone	wackestone	-1.87	-7.28	Darriwilian	Sand Shoal Complex	Ope
Antelope Valley Limestone	ACO-28	28	bioclastic wackestone, thin mud interbeds, sparse chert	wackestone	-1.69	-7.32	Darriwilian	Sand Shoal Complex	Ope
Antelope Valley Limestone	ACO-28.2	28.2	oncolitic packstone	packstone	-1.94	-7.32	Darriwilian	Sand Shoal Complex	Ope
Antelope Valley Limestone	ACO-30	30	bioclastic wackestone, thin mud interbeds, sparse chert	wackestone	-1.72	-7.06	Darriwilian	Sand Shoal Complex	Ope
Antelope Valley Limestone	ACO-31	31	oncolitic packstone, shaly partings	packstone	-1.82	-7.53	Darriwilian	Sand Shoal Complex	Ope
Antelope Valley Limestone	ACO-32.2	32.2	oncolitic packstone-wackstone, shaly partings	packstone-wackestone	-1.66	-7.09	Darriwilian	Sand Shoal Complex	Ope
Antelope Valley Limestone	ACO-33.1	33.1	oncolitic packstone-wackstone, shaley partings	packstone-wackestone	-1.65	-7.02	Darriwilian	Sand Shoal Complex	Ope

Antelope Valley Limestone	ACO-34.2	34.2	oncolitic-bioclastic wackestone	wackestone	-1.29	-6.51	Darriwilian	Sand Shoal Complex	Ope
Antelope Valley Limestone	ACO-35	35	oncolitic wackestone	wackestone	-1.62	-7.14	Darriwilian	Sand Shoal Complex	Ope
Antelope Valley Limestone	ACO-36	36	oncolitic-bioclastic wackestone	wackestone	-1.85	-7.65	Darriwilian	Sand Shoal Complex	Ope
Antelope Valley Limestone	ACO-36.6	36.6	oncolitic-bioclastic wackestone	wackestone	-1.75	-6.98	Darriwilian	Sand Shoal Complex	Ope
Antelope Valley Limestone	ACO-37	37	bioclastic wackestone with thin mud interbeds	wackestone	-1.60	-7.03	Darriwilian	Sand Shoal Complex	Ope
Antelope Valley Limestone	ACO-38	38	bioclastic wackestone with thin mud interbeds	wackestone	-1.58	-6.97	Darriwilian	Sand Shoal Complex	Ope
Antelope Valley Limestone	ACO-38.7	38.7	oncolitic-bioclastic packstone	packstone	-1.86	-7.66	Darriwilian	Sand Shoal Complex	Ope
Antelope Valley Limestone	ACO-41	41	Bioclastic packstone-wackestone with thin mud interbeds	packstone-wackestone	-1.70	-7.02	Darriwilian	Sand Shoal Complex	Ope
Antelope Valley Limestone	ACO-42	42	Bioclastic packstone-wackestone with thin mud interbeds	packstone	-1.48	-7.28	Darriwilian	Sand Shoal Complex	Ope
Antelope Valley Limestone	ACO-43	43	oncolitic-bioclastic packstone-grainstone, med.gray, thin tan mud beds	packstone-grainstone	-1.61	-7.72	Darriwilian	Sand Shoal Complex	Ope
Antelope Valley Limestone	ACO-44.2	44.2	oncolitic packstone, muddy oncolites, med-dark gray	packstone	-1.98	-8.60	Darriwilian	Sand Shoal Complex	Ope
Antelope Valley Limestone	ACO-45	45	oncolitic-bioclastic packstone-wackestone, shaley partings, med.gray, thin red mud	packstone-wackestone	-1.48	-7.78	Darriwilian	Sand Shoal Complex	Ope
Antelope Valley Limestone	ACO-46	46	oncolitic packstone, med.gray, pure calcite face, tan mud, birds eye voids	packstone	-1.55	-8.01	Darriwilian	Sand Shoal Complex	Ope

Antelope Valley Limestone	ACO-47.2	47.2	oncolitic packstone, med.gray, very small voids	packstone	-1.34	-7.10	Darriwilian	Sand Shoal Complex	Ope
Antelope Valley Limestone	ACO-48	48	oncolitic-bioclastic wackestone, med-dark gray, peloids, tan mud	wackestone	-1.23	-6.83	Darriwilian	Sand Shoal Complex	Ope
Antelope Valley Limestone	ACO-49.2	49.2	oncolitic packstone,thin shaley partings med.gray, orange mud	packstone	-1.38	-8.30	Darriwilian	Sand Shoal Complex	Ope
Antelope Valley Limestone	ACO-50.1	50.1	oncolitic-bioclastic packstone, med-dark gray, peloids	packstone	-1.29	-7.06	Darriwilian	Sand Shoal Complex	Ope
Antelope Valley Limestone	ACO-51	51	oncolitic-bioclastic grainstone, med.gray, red & tan mud	grainstone	-1.14	-6.94	Darriwilian	Sand Shoal Complex	Ope
Antelope Valley Limestone	ACO-52	52	oncolitic-bioclastic packstone-grainstone with shaley partings, med-dark gray, red mud	packstone-grainstone	-1.47	-7.64	Darriwilian	Sand Shoal Complex	Ope
Antelope Valley Limestone	ACO-53.2	53.2	oncolitic-bioclastic packstone-grainstone, med.gray, tan mud, bioturbated	packstone-grainstone	-1.41	-6.92	Darriwilian	Sand Shoal Complex	Ope
Antelope Valley Limestone	ACO-54.2	54.2	oncolitic packstone-wackestone,ooids, med.gray, tan mud, peloids	packstone-wackestone	-1.07	-6.68	Darriwilian	Sand Shoal Complex	Ope
Antelope Valley Limestone	ACO-55	55	oncolitic-oolitic grainstone,med-dark gray, tan mud, peloids, some big blocky calcite	grainstone	-1.31	-6.96	Darriwilian	Sand Shoal Complex	Ope
Antelope Valley Limestone	ACO-56	56	oncolitic-bioclastic packstone-wackestone, med.gray, peloids	packstone-wackestone	-1.34	-6.65	Darriwilian	Sand Shoal Complex	Opf
Antelope Valley Limestone	ACO-56.2	56.2	oolitic packstone-wackestone, med.gray, tan & orange mud, splotchy blocky calcite	packstone-wackestone	-1.13	-6.51	Darriwilian	Sand Shoal Complex	Opf
Antelope Valley Limestone	ACO-57	57	oolitic-bioclastic grainstone, med-dark gray, tan mud	grainstone	-1.64	-7.13	Darriwilian	Sand Shoal Complex	Opf

Antelope Valley Limestone	ACO-58	58	oolitic-bioclastic grainstone, med.gray, tan and red mud, birds eye voids	grainstone	-1.56	-6.27	Darriwilian	Sand Shoal Complex	Opf
Antelope Valley Limestone	ACO-60	60	oncolitic packstone, med.gray, tan and red mud, birds eye voids	packstone	-1.99	-7.25	Darriwilian	Sand Shoal Complex	Opf
Antelope Valley Limestone	ACO-61	61	bioclastic packstone-wackestone, med.gray,med. Crystalline, red and orange mud	packstone-wackestone	-2.23	-7.08	Darriwilian	Sand Shoal Complex	Opf
Antelope Valley Limestone	ACO-62	62	oolitic-bioclastic grainstone, med.gray,med. Crystalline, red and orange mud, calcite veins	grainstone	-2.42	-7.46	Darriwilian	Sand Shoal Complex	Opf
Antelope Valley Limestone	ACO-63.1	63.1	oncolitic grainstone, med.gray, red mud vein	grainstone	-1.71	-6.92	Darriwilian	Sand Shoal Complex	Opf
Antelope Valley Limestone	ACO-64.3	64.3	oncolitic packstone, med.gray, oxidized brach shell	packstone	-1.93	-7.14	Darriwilian	Sand Shoal Complex	Opf
Antelope Valley Limestone	ACO-65	65	oncolitic-oolitic grainstone, med.dark gray	grainstone	-2.04	-7.42	Darriwilian	Sand Shoal Complex	Opf
Antelope Valley Limestone	ACO-66.2	66.2	oncolitic wackestone, med.dark gray, minor blocky calcite	wackestone	-1.78	-7.14	Darriwilian	Sand Shoal Complex	Opf
Antelope Valley Limestone	ACO-67.2	67.2	oncolitic wackestone, med.gray, tan mud	wackestone	-1.84	-7.11	Darriwilian	Sand Shoal Complex	Opf
Antelope Valley Limestone	ACO-68.1	68.1	oncolitic-oolitic-grainstone, med.dark gray, calcite vein, red oxidized oncoid,	grainstone	-1.82	-7.19	Darriwilian	Sand Shoal Complex	Opf
Antelope Valley Limestone	ACO-69	69	oncolitic-oolitic grainstone, med.dark gray, tan mud, tan oxidized oncoid	grainstone	-1.87	-7.58	Darriwilian	Sand Shoal Complex	Opf
Antelope Valley Limestone	ACO-70.1	70.1	oncolitic wackestone, med.dark gray, tan mud, red oxidized oncoid	wackestone	-1.95	-7.09	Darriwilian	Sand Shoal Complex	Opf

Antelope Valley Limestone	ACO-71.0	71	oolitic-bioclastic grainstone-packstone, shaley partings, med.gray, tan mud, peloids	packstone-grainstone	-1.58	-6.87	Darriwilian	Sand Shoal Complex	Opf
Antelope Valley Limestone	ACO-72.4	72.4	oncolitic-oolitic grainstone, med.dark gray, red mud, partially silicified	grainstone	-1.73	-6.80	Darriwilian	Sand Shoal Complex	Opf
Antelope Valley Limestone	ACO-73.2	73.2	oncolitic-oolitic grainstone, med.gray, peloids, chert, iron oxides	grainstone	-1.90	-7.02	Darriwilian	Sand Shoal Complex	Opf
Antelope Valley Limestone	ACO-74.2	74.2	oncolitic-oolitic grainstone-packstone, med.gray, tan mud, peloids	grainstone-packstone	-1.50	-6.62	Darriwilian	Sand Shoal Complex	Opf
Antelope Valley Limestone	ACO-75.4	75.4	oncolitic-oolitic grainstone-packstone, med.gray, tan mud lenses,peloids tan oncoid, iron orange calcite	grainstone-packstone	-1.68	-6.57	Darriwilian	Sand Shoal Complex	Opf
Antelope Valley Limestone	ACO-76	76	oncolitic-oolitic grainstone, med.gray, peloids, minor red mud	grainstone	-1.49	-6.58	Darriwilian	Sand Shoal Complex	Opf
Antelope Valley Limestone	ACO-77	77	oncolitic-oolitic grainstone-packstone, med.gray, erosional base	grainstone-packstone	-1.50	-6.69	Darriwilian	Sand Shoal Complex	Opf
Antelope Valley Limestone	ACO-78	78	bioclastic wackestone, med.gray, tan oncoid, minor peloids	wackestone	-1.69	-6.31	Darriwilian	Sand Shoal Complex	Opf
Antelope Valley Limestone	ACO-78	78	Oncolitic-oolitic grain-packstone, med.gray, major peloids, light crystaline	grainstone	-1.76	-6.94	Darriwilian	Sand Shoal Complex	Opf
Antelope Valley Limestone	ACO-81	81	oncolitic grainstone, med.gray, minute calcite veins, slight caliche on weathered side	grainstone	-1.31	-6.58	Darriwilian	Sand Shoal Complex	Opf

Antelope Valley Limestone	ACO-82	82	bioclastic grainstone-packstone, med.gray, med crystalline, bioturbated,mud drapes	grainstone-packstone	-1.58	-6.89	Darriwilian	Sand Shoal Complex	Opf
Antelope Valley Limestone	ACO-83	83	packstone, med.gray	packstone	-1.60	-7.04	Darriwilian	Shallow Lagoon	Opf
Antelope Valley Limestone	ACO-84	84	intraclastic-oolitic grainstone, med.gray, heavy crystalline, caliche side	grainstone	-1.68	-7.06	Darriwilian	Shallow Lagoon	Opf
Antelope Valley Limestone	ACO-85	85	oncolitic packstone, med.gray, oxidized oncolites, tan mud lense	packstone	-1.59	-7.04	Darriwilian	Shallow Lagoon	Opf
Antelope Valley Limestone	ACO-86	86	lime mudstone, light gray, mod-heavy crystalline, tan mud lens	lime mudstone	-2.10	-7.46	Darriwilian	Shallow Lagoon	Opf
Antelope Valley Limestone	ACO-87	87	bioclastic-oolitic grainstone, med.gray, red mud lens, peloids?	grainstone	-1.40	-7.34	Darriwilian	Shallow Lagoon	Opf
Antelope Valley Limestone	ACO-88	88	bioclastic-oolitic grainstone, med.gray, red mud lens, peloids	grainstone	-1.33	-7.12	Darriwilian	Shallow Lagoon	Opf
Antelope Valley Limestone	ACO-89	89	lime mudstone, med.gray, tan mud lenses,	lime mudstone	-1.34	-7.16	Darriwilian	Shallow Lagoon	Opf
Antelope Valley Limestone	ACO-90	90	lime mudstone, med.gray, red mud lenses	lime mudstone	-1.45	-7.21	Darriwilian	Shallow Lagoon	Opf
Antelope Valley Limestone	ACO-91	91	oolitic-bioclastic grainstone, light gray, mod. crystalline, peloids?	grainstone	-1.27	-6.61	Darriwilian	Shallow Lagoon	Opf
Antelope Valley Limestone	ACO-92	92	bioclastic packstone, med.gray, red mud drapes, minor blocky calcite,	packstone	-1.18	-7.18	Darriwilian	Shallow Lagoon	Opf
Antelope Valley Limestone	ACO-93.1	93.1	bioclastic grainstone, med.gray, heavy tan mud,	grainstone	-1.37	-6.40	Darriwilian	Shallow Lagoon	Opf

Antelope Valley Limestone	ACO-94	94	bioclastic grainstone,med.gray, heavy mud	grainstone	-1.53	-7.06	Darriwilian	Shallow Lagoon	Opf
Antelope Valley Limestone	ACO-94.2	94.2	bioclastic-intraclastic grainstone, Light gray, minor red mud lens, brach frag shells	grainstone	-1.15	-6.83	Darriwilian	Shallow Lagoon	Opf
Antelope Valley Limestone	ACO-95	95	muddy packstone with mud drapes, light gray & red oxides,	packstone	-1.31	-7.18	Darriwilian	Shallow Lagoon	Opf
Antelope Valley Limestone	ACO-96.3	96.3	oncolitic-oolitic grainstone,light grey, coarse crystalline, red oxides	grainstone	-1.38	-6.75	Darriwilian	Shallow Lagoon	Opf
Antelope Valley Limestone	ACO-97.4A	97.4	intraclastic-bioclastic grainstone,med. gray, tan mud lens	grainstone	-1.33	-6.33	Darriwilian	Shallow Lagoon	Opf
Antelope Valley Limestone	ACO-98.1	98.1	grainstone,light grey, med. crystalline, red oxides, tan mud	grainstone	-1.79	-6.41	Darriwilian	Shallow Lagoon	Opf
Antelope Valley Limestone	ACO-100.0	100	bioclastic packstone,light grey, med.-coarse crystalline, red oxides, tan and red mud lens,	packstone	-2.51	-6.42	Darriwilian	Shallow Lagoon	Opf
Antelope Valley Limestone	ACO-101.0	101	bioclastic packstone,Light gray, med. crystalline, red oxides, tan mud	packstone	-1.70	-6.45	Darriwilian	Shallow Lagoon	Opf
Antelope Valley Limestone	ACO-102.0	102	bioclastic grainstone,dark gray, min. red&tan mud	grainstone	-1.18	-6.49	Darriwilian	Shallow Lagoon	Opf
Antelope Valley Limestone	ACO-103.2	103.2	bioclastic grainstone, light-med.gray, med. crystalline, sparse mud	grainstone	-1.52	-6.20	Darriwilian	Shallow Lagoon	Opf
Antelope Valley Limestone	ACO-104.1	104.1	bioclastic packstone-grainstone with thin red mud lenses, abundant Recep., med.gray, fine crystalline, red mud	packstone-grainstone	-1.87	-6.67	Darriwilian	Shallow Lagoon	Opf

Antelope Valley Limestone	ACO-105.0	105	bioclastic packstone,med.gray,v. fine crystalline, red&tan mud drapes	packstone	-1.70	-7.07	Darriwilian	Shallow Lagoon	Opf
Antelope Valley Limestone	ACO-106.0	106	bioclastic packstone-grainstone with thin mud, med.gray,v. fine crystalline, sparse red&tan mud	packstone-grainstone	-1.73	-6.66	Darriwilian	Shallow Lagoon	Opf
Antelope Valley Limestone	ACO-107.3	107.3	Mudstone interbedded with bioclastic pack-wackestone, med.gray, fine crystalline, purple&tan mud	lime mudstone	-1.71	-6.48	Darriwilian	Shallow Lagoon	Opf
Antelope Valley Limestone	ACO-108.0	108	Mudstone interbedded with bioclastic pack-wackestone, med.gray, fine crystalline, sparse purple mud	lime mudstone	-1.80	-6.63	Darriwilian	Shallow Lagoon	Opf
Antelope Valley Limestone	ACO-109.0	109	oncolitic wackestone-packstone with mud and abundant Recept., med.gray, fine crystalline, tan mud	wackestone	-2.15	-7.33	Darriwilian	Shallow Lagoon	Opf
Antelope Valley Limestone	ACO-110.0	110	oncolitic wackestone with mud and abundant Recept.,med.gray,v. fine crystalline, red&tan mud	wackestone	-2.22	-6.48	Darriwilian	Shallow Lagoon	Opf
Antelope Valley Limestone	ACO-111.1	111.1	bioclastic-oncolitic packstone-grainstone, abundant Recept., med.gray,v. fine crystalline, red&tan mud	packstone-grainstone	-2.39	-6.33	Darriwilian	Shallow Lagoon	Opf
Antelope Valley Limestone	ACO-112.0	112	bioclastic oncolitic packstone-wackestone, med.gray,v. fine crystalline, purple mud	packstone-wackestone	-2.67	-6.42	Darriwilian	Tidal Flat	Opf

Antelope Valley Limestone	ACO-113.0	113	bioclastic wackestone with mud, med.gray,v. fine crystalline, purple mud	wackestone	-2.07	-6.36	Darriwilian	Tidal Flat	Opf
Antelope Valley Limestone	ACO-114.0	114	Oolitic grainstone with crossbeds and siliciclastic drapes, med.gray,v. fine crystalline, sparse red&tan mud	grainstone	-1.47	-6.42	Darriwilian	Tidal Flat	Opf
Antelope Valley Limestone	ACO-115.0	115	oolitic-peloidal grainstone, med.gray, fine crystalline, sparse red&tan mud	grainstone	-1.28	-5.96	Darriwilian	Tidal Flat	Opf
Antelope Valley Limestone	ACO-116.1	116.1	calcareous siltstone, med.gray, fine crystalline, sparse red&tan mud	calcareous siltstone	-1.60	-6.41	Darriwilian	Tidal Flat	Opf
Antelope Valley Limestone	ACO-117	117	silty mudstone interbedded with peloidal wackestone-packstone, light gray, microcrystalline	lime mudstone	-1.76	-6.23	Darriwilian	Tidal Flat	Opf
Antelope Valley Limestone	ACO-118	118	silty mudstone interbedded with peloidal wackestone-packstone, med.gray, v.fine crystalline, thin mud	lime mudstone	-2.67	-6.22	Darriwilian	Tidal Flat	Opf
Antelope Valley Limestone	ACO-119.3	119.3	peloidal bioclastic wackestone-packstone, med.-dark gray, v.fine crystalline, purple mud lens	wackestone-packstone	-2.59	-6.54	Darriwilian	Tidal Flat	Opf
Antelope Valley Limestone	ACO-120	120	bioclastic wackestone-packstone, med.-dark gray, fine-med. crystalline, purple mud lens	wackestone-packstone	-3.20	-6.42	Darriwilian	Tidal Flat	Opf
Antelope Valley Limestone	ACO-121	121	bioclastic wackestone-packstone, med.-dark gray, fine-med. crystalline, purple mud lens	wackestone-packstone	-3.44	-6.81	Darriwilian	Tidal Flat	Opf

Antelope Valley Limestone	ACO-122.4	122.4	packstone, med.gray,microcrystalline, red&tan mud,	packstone	-3.58	-6.39	Darriwilian	Tidal Flat	Opf
Antelope Valley Limestone	ACO-123.2	123.2	cryptic lime-mudstone, med.gray,microcrystalline, tan mud,	lime mudstone	-3.01	-6.19	Darriwilian	Tidal Flat	Opf
Antelope Valley Limestone	ACO-124.0	124	cryptic lime-mudstone, med.gray,microcrystalline, tan mud,	lime mudstone	-2.97	-6.06	Darriwilian	Tidal Flat	Opf
Antelope Valley Limestone	ACO-125.0	125	bioclastic packstone-wackestone, dark gray, microcrystalline, sparse tan mud	wackestone	-4.59	-6.64	Darriwilian	Tidal Flat	Opf
Antelope Valley Limestone	ACO-126.0	126	grainstone, dark gray, microcrystalline, sparse tan mud,	grainstone	-4.78	-6.40	Darriwilian	Tidal Flat	Opf
Antelope Valley Limestone	ACO-127.1	127.1	wackestone with mudstone interbeds, dark gray, microcrystalline, tan mud,	wackestone	-1.83	-6.50	Darriwilian	Tidal Flat	Opf
Antelope Valley Limestone	ACO-128.0	128	wackestone with mudstone interbeds, dark gray, microcrystalline, tan mud,	lime mudstone	-2.23	-6.26	Darriwilian	Tidal Flat	Opf
Antelope Valley Limestone	ACO-129.0	129	oncolitic grainstone, med.-dark gray, v.fine crystalline, purple mud lens	grainstone	-3.94	-6.30	Darriwilian	Tidal Flat	Opf
Antelope Valley Limestone	ACO-130.0	130	cryptic lime mudstone with microbial laminae, light gray, microcrystalline	lime mudstone	-2.45	-5.94	Darriwilian	Tidal Flat	Opf
Antelope Valley Limestone	ACO-131.0	131	cryptic lime mudstone with microbial laminae, light gray, microcrystalline	lime mudstone	-2.45	-6.08	Darriwilian	Tidal Flat	Opf
Antelope Valley Limestone	ACO-132.3	132.3	intraclastic grainstone, med.gray, fine crystalline, red mud	grainstone	-3.43	-6.09	Darriwilian	Tidal Flat	Opf

Antelope Valley Limestone	ACO-133.0	133	lime-mudstone, med.gray, fine crystalline, red & tan mud	lime mudstone	-3.43	-6.34	Darriwilian	Tidal Flat	Opf
Antelope Valley Limestone	ACO-134.1	134.1	lime-mudstone, med.gray, fine crystalline, red & tan mud	lime mudstone	-3.15	-6.41	Darriwilian	Tidal Flat	Opf
Antelope Valley Limestone	ACO-135.1	135.1	Intraclastic bioclastic grainstone, med.gray,microcrystalline, tan mud	grainstone	-3.25	-7.02	Darriwilian	Tidal Flat	Opf
Antelope Valley Limestone	ACO-136.2	136.2	lime-mudstone, med. gray, red&tan mud lens, caliche side	lime mudstone	-2.78	-6.43	Darriwilian	Tidal Flat	Opf
Antelope Valley Limestone	ACO-137.1	137.1	wackestone interbedded with oncolitic packstone, med.gray, sparse mud, microcrystaline	wackestone	-4.26	-6.70	Darriwilian	Tidal Flat	Opf
Antelope Valley Limestone	ACO-138.0	138	bioclastic wackestone, med.gray, v.fine crystalline, purple mud	wackestone	-3.38	-5.93	Darriwilian	Tidal Flat	Opf
Antelope Valley Limestone	ACO-140.1	140.1	bioclastic wackestone, med.gray, v.fine crystalline, tan&pink mud	wackestone-mudstone	-2.76	-6.38	Darriwilian	Tidal Flat	Opf
Antelope Valley Limestone	ACO-141.1	141.1	peloidal-oolitic grainstone, med.gray, fine crystalline, tan mud	grainstone	-5.44	-6.61	Darriwilian	Tidal Flat	Opf
Antelope Valley Limestone	ACO-142.0	142	lime-mudstone, med.gray, fine crystalline, tan mud	lime mudstone	-3.81	-6.28	Darriwilian	Tidal Flat	Opf
Antelope Valley Limestone	ACO-143.0	143	lime mudstone, med.-dark gray, microcrystalline, rare mud	lime mudstone	-2.44	-6.19	Darriwilian	Tidal Flat	Opf
Antelope Valley Limestone	ACO-144.0	144	lime mudstone, med.dark gray, purple mud lens	lime mudstone	-2.95	-6.12	Darriwilian	Tidal Flat	Opf

Antelope Valley Limestone	ACO-145.0	145	oolitic grainstone,med.dark gray, microcrystalline	grainstone	-1.86	-6.37	Darriwilian	Tidal Flat	Opf
Antelope Valley Limestone	ACO-146.0	146	dolomitic lime-mudstone, med. gray,microcrystalline	lime mudstone	-2.76	-4.52	Darriwilian	Tidal Flat	Opf
Antelope Valley Limestone	ACO-147.0	147	intraclastic bioclastic grainstone-packstone, med.gray, microcrystalline,	grainstone-packstone	-3.31	-6.17	Darriwilian	Tidal Flat	Opf
Antelope Valley Limestone	ACO-148.0	148	intraclastic bioclastic grainstone-packstone, med.gray, microcrystalline,	grainstone-packstone	-3.01	-4.43	Darriwilian	Tidal Flat	Opf
Antelope Valley Limestone	ACO-149.0	149	lime-mudstone, med.gray, microcrystalline,	lime mudstone	-3.21	-5.99	Darriwilian	Tidal Flat	Opf
Antelope Valley Limestone	ACO-150.0	150	wackestone with cryptic laminae, light gray, microcrystalline	wackestone	-3.10	-5.52	Darriwilian	Tidal Flat	Opf
Antelope Valley Limestone	ACO-151.0	151	wackestone with cryptic laminae, light gray, microcrystalline thin tan mud	wackestone	-2.99	-6.67	Darriwilian	Tidal Flat	Opf
Antelope Valley Limestone	ACO-152.0	152	lime-mudstone, med.-darkgray, v.fine crystalline	lime mudstone	-5.14	-6.47	Darriwilian	Tidal Flat	Opf
Antelope Valley Limestone	ACO-153.0	153	muddy bioclastic packstone, med.-darkgray, v.fine crystalline	packstone	-3.11	-7.31	Darriwilian	Tidal Flat	Opf
Antelope Valley Limestone	ACO-154.0	154	mudstone, very light gray, microcrystalline, some tan mud	lime mudstone	-3.88	-6.99	Darriwilian	Tidal Flat	Opf
Antelope Valley Limestone	ACO-155.0	155	bioclastic grainstone, med.gray, fine crystalline	grainstone	-5.09	-6.57	Darriwilian	Tidal Flat	Opf
Antelope Valley Limestone	ACO-156.0	156	bioclastic packstone, med.gray, fine-med. Crystalline	packstone	-4.50	-6.28	Darriwilian	Tidal Flat	Opf

Antelope Valley Limestone	ACO-157.0	157	bioclastic packstone, med.-dark gray, v.fine crystalline, purple mud lens	packstone	-2.55	-6.39	Darriwilian	Tidal Flat	Opf
Antelope Valley Limestone	ACO-158.0	158	lime mudstone, med.-dark gray, v.fine crystalline,	lime mudstone	-1.36	-6.43	Darriwilian	Tidal Flat	Opf
Antelope Valley Limestone	ACO-159.0	159	intraclastic packstone, med.-dark gray, v.fine crystalline, purple&tan mud	packstone	-2.85	-6.32	Darriwilian	Tidal Flat	Opf
Antelope Valley Limestone	ACO-160.0	160	bioclastic wackestone,med.-dark gray, v.fine crystalline, tan mud	wackestone	-3.43	-7.03	Darriwilian	Tidal Flat	Opf
Antelope Valley Limestone	ACO-161.0	161	wackestone,med.gray, v.fine crystalline, tan mud	wackestone	-2.90	-6.48	Darriwilian	Tidal Flat	Opf
Antelope Valley Limestone	ACO-162.0	162	bioclastic wackestone-packstone, lt.-med. gray, v.fine crystalline, gray mud	wackestone-packstone	-2.15	-5.78	Darriwilian	Tidal Flat	Opf
Antelope Valley Limestone	ACO-163.0	163	grainstone, lt.-med. gray, v.fine crystalline, gray mud	grainstone	-2.18	-6.29	Darriwilian	Tidal Flat	Opf
Antelope Valley Limestone	ACO-164.0	164	bioclastic grainstone with erosional base, med.gray, v.fine crystalline, tan mud	grainstone	-2.66	-5.66	Darriwilian	Tidal Flat	Opf
Antelope Valley Limestone	ACO-165.0	165	wackestone-mudstone, dark gray, microcrystalline, rare mud	wackestone-mudstone	-4.08	-6.43	Darriwilian	Tidal Flat	Opf
Antelope Valley Limestone	ACO-166.0	166	intraclastic bioclastic grainstone-[ackstone, med.gray, v.fine crystalline, minor tan mud	grainstone-packstone	-4.36	-6.09	Darriwilian	Tidal Flat	Opf
Antelope Valley Limestone	ACO-167.0	167	lime-mudstone, dark gray, microcrystalline, rare mud	lime mudstone	-2.97	-7.69	Darriwilian	Tidal Flat	Opf

Antelope Valley Limestone	ACO-168.0	168	lime mudstone, med.-dark gray, microcrystalline, rare mud	lime mudstone	-2.80	-7.27	Darriwilian	Tidal Flat	Opf
Antelope Valley Limestone	ACO-169.0	169	wackestone-packstone, med.-dark gray, microcrystalline, rare mud	wackestone-packstone	-2.41	-7.52	Darriwilian	Tidal Flat	Opf
Antelope Valley Limestone	ACO-170.0	170	bioclastic-oolitic grainstone, med.gray, v.fine crystalline, minor tan mud	grainstone	-3.17	-6.62	Darriwilian	Tidal Flat	Opf
Antelope Valley Limestone	ACO-171.0	171	wackestone-mudstone, med.-dark gray, v.fine crystalline, minor tan mud	wackestone-mudstone	-3.44	-7.18	Darriwilian	Tidal Flat	Opf
Antelope Valley Limestone	ACO-172.0	172	dolostone,med.-dark gray, fine crystalline, rare tan mud	dolostone	-3.31	-4.35	Darriwilian	Tidal Flat	Opf
Antelope Valley Limestone	ACO-173.0	173	dolostone,med.-dark gray, fine-med. crystalline, rare tan mud	dolostone	-2.94	-2.98	Darriwilian	Tidal Flat	Opf
Antelope Valley Limestone	ACO-174.0	174	dolostone,med.-dark gray, fine-med. crystalline, rare tan mud	dolostone	-2.61	-2.29	Darriwilian	Tidal Flat	Opf
Antelope Valley Limestone	ACO-175.6	175.6	dolostone,med.-dark gray, fine-med. crystalline, rare tan mud	dolostone	-2.23	-2.44	Darriwilian	Tidal Flat	Opf
Antelope Valley Limestone	ACO-177.0	177	dolostone,med.-dark gray, fine-med. crystalline, rare tan mud	dolostone	-1.72	-2.32	Darriwilian	Tidal Flat	Opf
Antelope Valley Limestone	ACO-178.0	178	dolostone,med.-dark gray, fine-med. crystalline,	dolostone	0.06	-4.27	Darriwilian	Tidal Flat	Opf
Antelope Valley Limestone	ACO-179.0	179	dolostone,med.-dark gray, fine-med. crystalline, large quartz clast	dolostone	-1.79	-1.95	Darriwilian	Tidal Flat	Opf
Antelope Valley Limestone	ACO-180.0	180	dolostone,med.gray, fine crystalline, rare gray mud	dolostone	-2.18	-1.97	Darriwilian	Tidal Flat	Opf

Antelope Valley Limestone	ACO-181.0	181	dolostone,med.gray, fine crystalline, rare gray mud	dolostone	-2.03	-2.18	Darriwilian	Tidal Flat	Opf
Antelope Valley Limestone	ACO-182.2	182.2	dolostone,light-med.gray, fine crystalline,	dolostone	-2.03	-1.10	Darriwilian	Tidal Flat	Opf
Antelope Valley Limestone	ACO-182.6	182.6	dolostone,med.gray, fine crystalline,bioturbated	dolostone	-1.92	-0.86	Darriwilian	Tidal Flat	Opf
Antelope Valley Limestone	ACO-183.0	183	dolostone,med.gray, fine crystalline, bioturbated	dolostone	-2.19	-0.64	Darriwilian	Tidal Flat	Opf
Antelope Valley Limestone	ACO-184.0	184	dolostone,med.gray, fine crystalline, tan mud, dissolution voids	dolostone	-2.19	-2.26	Darriwilian	Tidal Flat	Opf

FIGURE CAPTIONS

Figure 1. Location of study section. **(A)** Middle-Late Ordovician global reconstruction showing the paleolatitude of Laurentia (modified from Scotese and McKerrow, 1990) and location of the Great Basin (green star). (B) Location of the study section (green star) and other sections studied by previous researchers. 1. Nopah Range, CA; 2. Sheep Range, NV; 3. Pahranagat Range, NV; 4. Hot Creek Range, NV; 5. Monitor Range, NV; 6. Shingle Pass, NV; 7. Ibex Hills, UT.

Figure 2. Location of the study section in the Arrow Canyon Range.

Figure 3. Generalized Ordovician stratigraphic units in the Arrow Canyon Range. A major unconformity is assumed between the Eureka Quartzite and the Antelope Valley Limestone (Cooper and Keller, 2001). The Copenhagen Formation is missing in the Arrow Canyon Range, along with the top of the Antelope Valley Limestone. The measured section covers the uppermost Antelope Valley Formation, in which *Receptaculites* sp. are abundant (Ope and Opf; Langenheim et al., 1962).

Figure 4. Middle-Late Ordovician (Darriwilian–Sandbian; ca. 467–453 Ma) carbonate carbon isotope profiles in Baltoscandia (Ainsaar et al., 2010), Monitor-Antelope Ranges (Saltzman et al., 2005a; Kump et al. 1999) and Shingle Pass/Ibex Hills (Edwards and Saltzman, 2014). The red line represents the unconformity. MDICE and Chatfieldian are positive excursions.

Figure 5. Variation of $\delta^{13}C$–$\delta^{18}O$ patterns in meteoric diagenetic environments (after Allan and Matthews, 1982). (**A**) $\delta^{13}C$–$\delta^{18}O$ pattern at exposure surface. (**B**) Large $\delta^{13}C$ but small $\delta^{18}O$ variations of meteoric diagenesis in general; (**C**) Negative $\delta^{13}C$ shift but

no significant $\delta^{18}O$ variation close to the water table. (**D**) Positive co-variance of $\delta^{13}C$ and $\delta^{18}O$ in mixing zone.

Figure 6. (A) Depositional model for the facies associations of the upper Antelope Valley Formation (or uppermost Ope and Opf of Langenheim et al. (1962)). The lower part of the measured section (0–95 m; Fig. 7) is dominated by oncolitic-oolitic shoal complex and tidal flat facies. The middle part (95–113 m; Fig. 7) consists mainly of mottled muddy limestone/wackestone and bioclastic packstone/grainstone deposited from shallow-lagoon environments. *Receptaculites* sp. is most abundant in this interval. The upper part of the measured section (113–184 m) show a decrease of grainstone/packstone and increase of lime mudstone and dolostone, which were likely deposited from proximal peritidal environments. The measured section (Fig. 7) records a progradational sequence. **(B)** Three types of meter-scale cycles recorded in the measured section. The sand shoal cycles consist of grainstone/packstone in the lower part and packstone with muddy drapes/lenses/thin laminae in the top. The shallow lagoon cycles are composed of packstone with muddy lenses/laminae in the lower part and wackestone/lime mudstone/mudstone in the upper part, in which bioclastic packstone lenses or thin beds may be found. The tidal flat cycles have packstone/grainstone at the base but are dominated by low-energy, fine-grained limestone and dolostone (lime mudstone, mudstone, wackestone), with thin lenses of packstone/grainstone. Mudcracks and dissolution cavities are found in some of the tidal flat cycles.

Figure 7. Measured stratigraphic column and carbon-oxygen isotope profile of the upper Antelope Valley Formation (uppermost Ope and Opf) in the Arrow Canyon Range. The lower portion of the stratigraphic column (0–113 m) has relatively "stable" $\delta^{13}C$ values

(mostly between -2‰ and -1‰). In contrast, the upper part of the section (114–184 m) close to the unconformity at base of the Eureka Quartzite shows large $\delta^{13}C$ fluctuations from -1‰ to -5.5‰, possibly related to diagenetic alternations.

Figure 8. Representative facies of the upper Antelope Valley Formation (Opf). (**A**) Thick-massive oncolitic grainstone facies (at 76 m). (**B**) Oncolitic-bioclastic packstone with thin (< 3 cm) mudstone/lime mudstone lenses (at 72 m). (**C**) Bioclastic wackestone with mudstone/lime mudstone lenses (at 104 m). (**D**) Interbedded mudstone/lime mudstone with packstone interbeds (at 86 m). (E) Intraclastic-bioclastic grainstone-packstone (at 115 m). (F) Dolomitic lime mudstone with dissolution cavities and mud drapes (at 171 m).

Figure 9. Well-preserved *Receptaculites* sp. and gastropods in lagoon facies association. (**A**) *Receptaculites* sp. preserved in bioclastic-oncolitic packstone with mudstone/lime mudstone lenses (Facies 3) at 106 m. (**B**) *Receptaculites* sp. and gastropods preserved in bioclastic-oncolitic wackestone with mudstone/lime mudstone lenses (Facies 4) at 104 m; (**C**) *Receptaculites* sp. and gastropods preserved in interbedded mudstone/lime mudstone with packstone interbeds (Facies 4) at 107 m; (**D**) *Receptaculites* sp. and gastropods preserved in bioclastic lime mudstone/mudstone (Facies 5) at 108 m.

Figure 10. Thin section photomicrographs of carbonate facies from the upper Antelope Valley Formation (Opf). (**A**) Oncolitic-oolitic grainstone of the sand shoal facies at 71 m. Only part of an oncoid (Onc) is shown in the right. Notice the present of calcite twins (CT) indicates burial diagenesis and deformation, but the thin twins suggest deformation temperature < 170°C (e.g., Burkhard, 1993; Paulsen et al., 2007). (**B**) Bioclastic-peloidal

grainstone of the sand shoal facies at 72 m. Thin calcite twins (CT) are observed. (**C**) Bioclastic wackestone with thin mudstone layers/lens of intertidal facies at 120 m. Significant amount (≤ 10%) of silt-sized quartz and feldspar are present in both wackestone and mudstone layers. (**D**) Intraclastic-bioclastic grainstone of shallow subtidal facies at 128 m. Bioclasts include fragments of brachiopods, trilobites, bryozoans and calcium microbes. (**E**) Dolomitic lime mudstone with cavities (CF) of intertidal-supratidal facies at 135 m. The cavity is filled with coarser-grained dolomite, silt, and mud. (**F**) Microcrystalline dolostone of supratidal facies at 183 m. Notice that both the fine-grained matrix and bioclasts are partially dolomitized. All photos were taken under plane-polarized light. Scale bar = 500 μm.

Figure 11. The $\delta^{13}C$–$\delta^{18}O$ crossplot vs. facies associations. Notice that the majority of samples have $\delta^{18}O$ values falling between –6‰ ~ –8‰ but a wide range of $\delta^{13}C$ from –5.5‰ to –0.4‰. The peritidal facies from 114m to 172 m have the most diverse $\delta^{13}C$ values (–1‰ to –5.5‰) but least variable $\delta^{18}O$ (–5.5‰ to -7.5‰). In contrast, the dolostone facies immediately below the Eureka Quartzite show a co-variation of $\delta^{13}C$ and $\delta^{18}O$.

Figure 12. The $\delta^{13}C$–$\delta^{18}O$ crossplot vs. lithologies. Except for the dolostones immediately below the Eureka Quartzite that show co-varying $\delta^{13}C$ and $\delta^{18}O$, there is no obvious lithology-dependent $\delta^{13}C$ and $\delta^{18}O$ trend.

Figure 13. The $\delta^{13}C$ and $\delta^{18}O$ variations in shallow lagoon and peritidal cycles. There is no significant or systematic change from the base to the top of cycles in these examples.

However, it should be pointed out that the current sample resolution is too low to test the meter-scale cycle-related isotope variations. Legends are the same as in Figure 6.

Figure 14. Carbon isotope variations below the Eureka Quartzite in the Great Basin (see Fig. 1 for location of sections). Negative $\delta^{13}C$ values down to ≤–5‰ are found in all measured sections but the depth of their occurrence below the basal Eureka Quartzite unconformity varies. In the Arrow Canyon Range section (this study), a negative $\delta^{13}C$ "excursion" (indicated by the dashed line) occurs 20–83 m below the unconformity. In Shingle Pass section (Edwards and Saltzman, 2014), $\delta^{13}C$ values show a minimum 80-100 m below the unconformity but low $\delta^{13}C$ values continue downwards. In Ibex Hills section (Edwards and Saltzman, 2014), a negative shift occur 0–50 below the Eureka Quartzite. In Pahranaghat Range section (Kosmidis, 2009), low (≤–2‰) $\delta^{13}C$ values are present 10–50 m below the Eureka Quartzite but in Hot Creek Range and Lone Mountain sections (Kosmidis, 2009), low (≤–2‰) $\delta^{13}C$ values appear only in strata 20–30 m below the Eureka Quartzite.

Figure 15. The $\delta^{13}C$–$\delta^{18}O$ crossplots of a few Middle Ordovician sections in the Great Basin (Nevada and Utah), with reference to the lithification and meteoric diagenetic trend (sky-blue band) of Knauth and Kennedy (2009). Each section below the Eureka Quartzite has points that plot along the meteoric diagenetic trend. (**A**) Arrow Canyon Range, Nevada (this study); (**B**) Monitor-Antelope Range, Nevada (Saltzman, 2005); (**C**) Shingle Pass, Nevada and Ibex Hills, Utah (Edwards and Saltzman, 2014); (**D**) Pahranaghat Range, Hot Creek Canyon, and Lone Mountain, Nevada (Kosmidis, 2009).

Figure 1

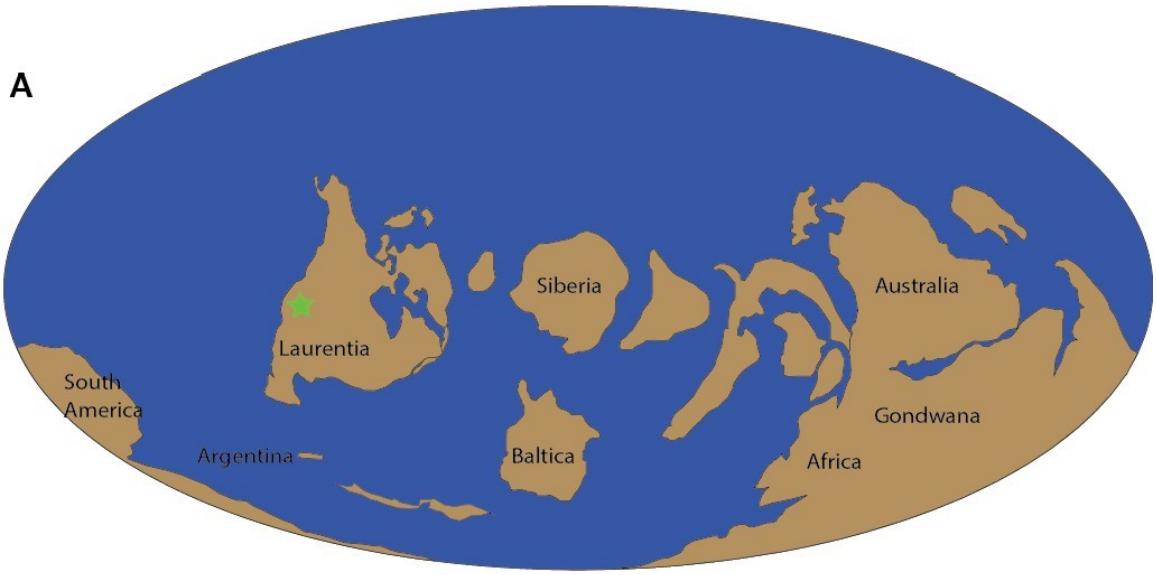
A
Siberia
Australia
Laurentia
South
America
Gondwana
Argentina
Baltica
Africa

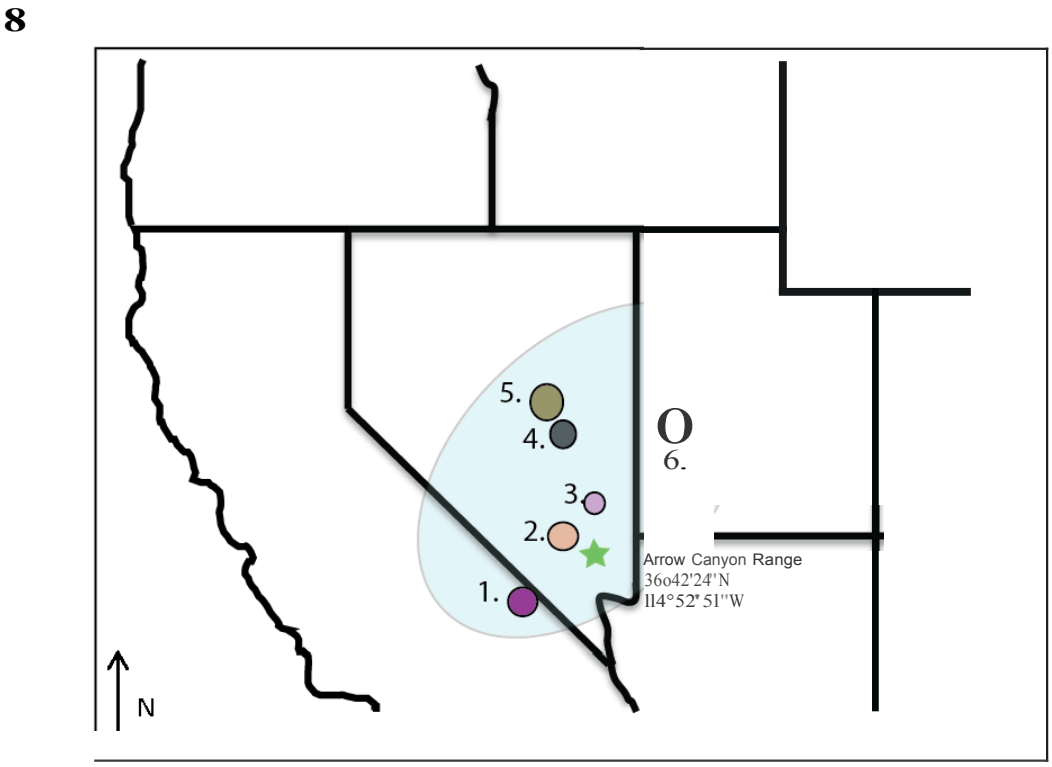
8
5.
4.
6.
3.
2.
1.
Arrow Canyon Range
36o42'24'N
II4°52' 51''W
N

Figure 2

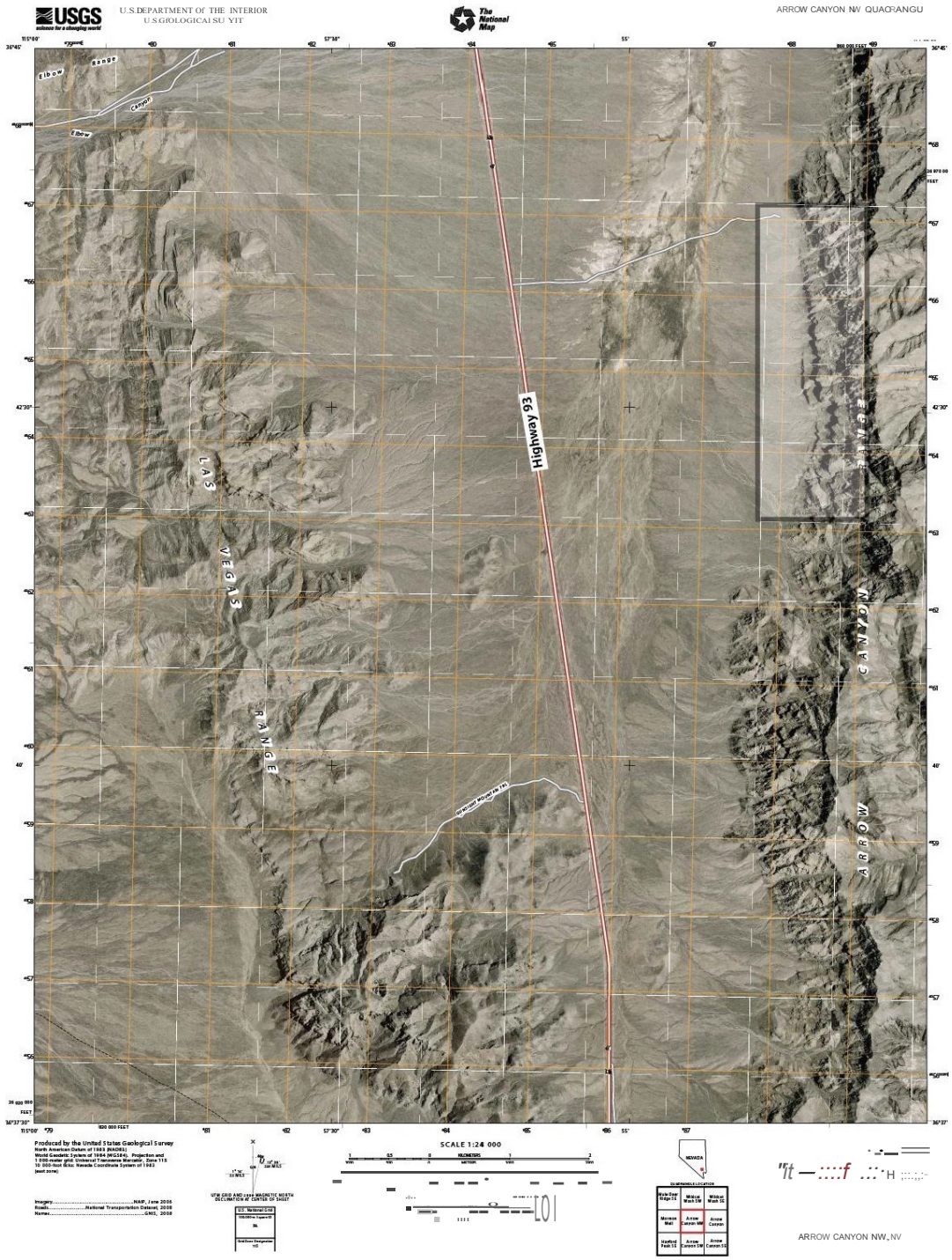
U.S.DEPARTMENT OF THE INTERIOR
U.S.GIOLOGICAI SU YIT
The National Map
ARROW CANYON NW QUACRANGU
Elbow
Canyon
Highway 93
LAS VEGAS RANGE
LAS VEGAS
RANGE
ARROW CANYON
ARROW
Produced by the United States Geological Survey
SCALE 1:24 000
NEVADA
ARROW CANYON NW, NV

Figure 3

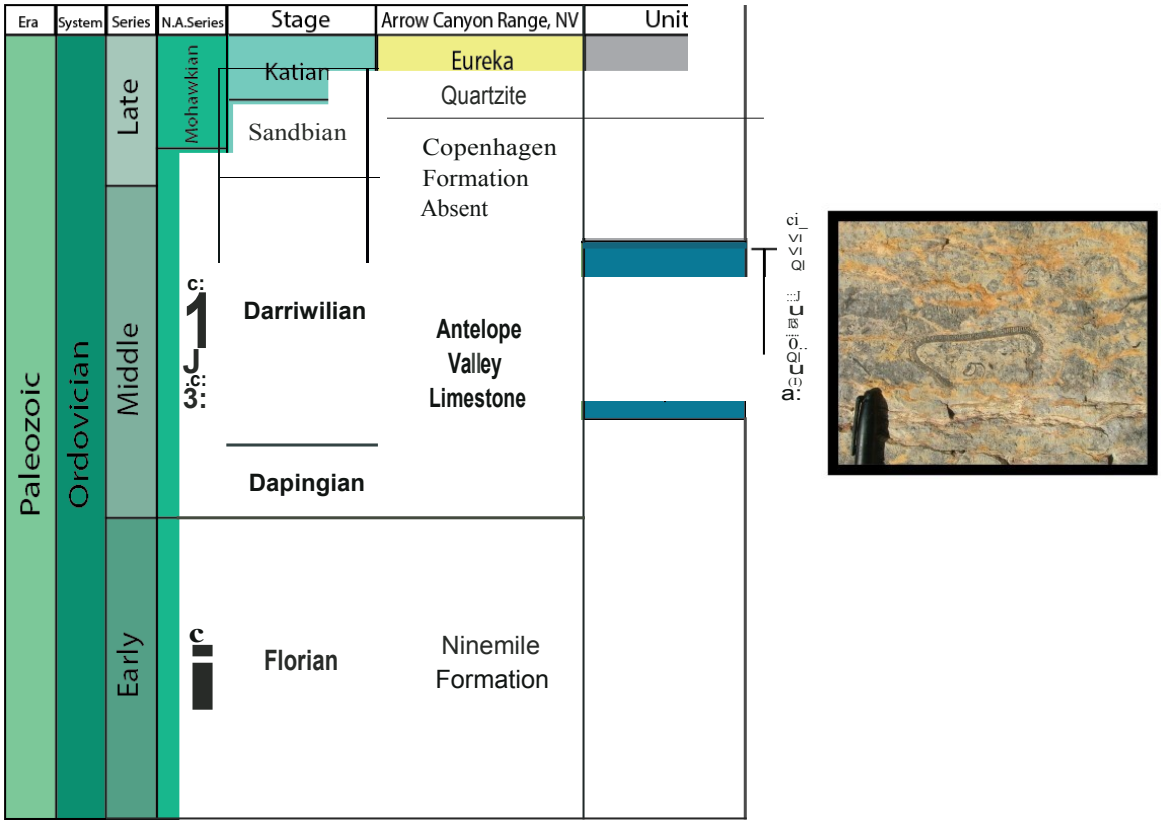
Era
System
Series
N.A.Series
Stage
Arrow Canyon Range, NV
Unit
Paleozoic
Ordovician
Late
Middle
Early
Mohawkian
Katian
Sandbian
Darriwilian
Dapingian
Florian
Eureka
Quartzite
Copenhagen
Formation
Absent
Antelope
Valley
Limestone
Ninemile
Formation

Figure 4

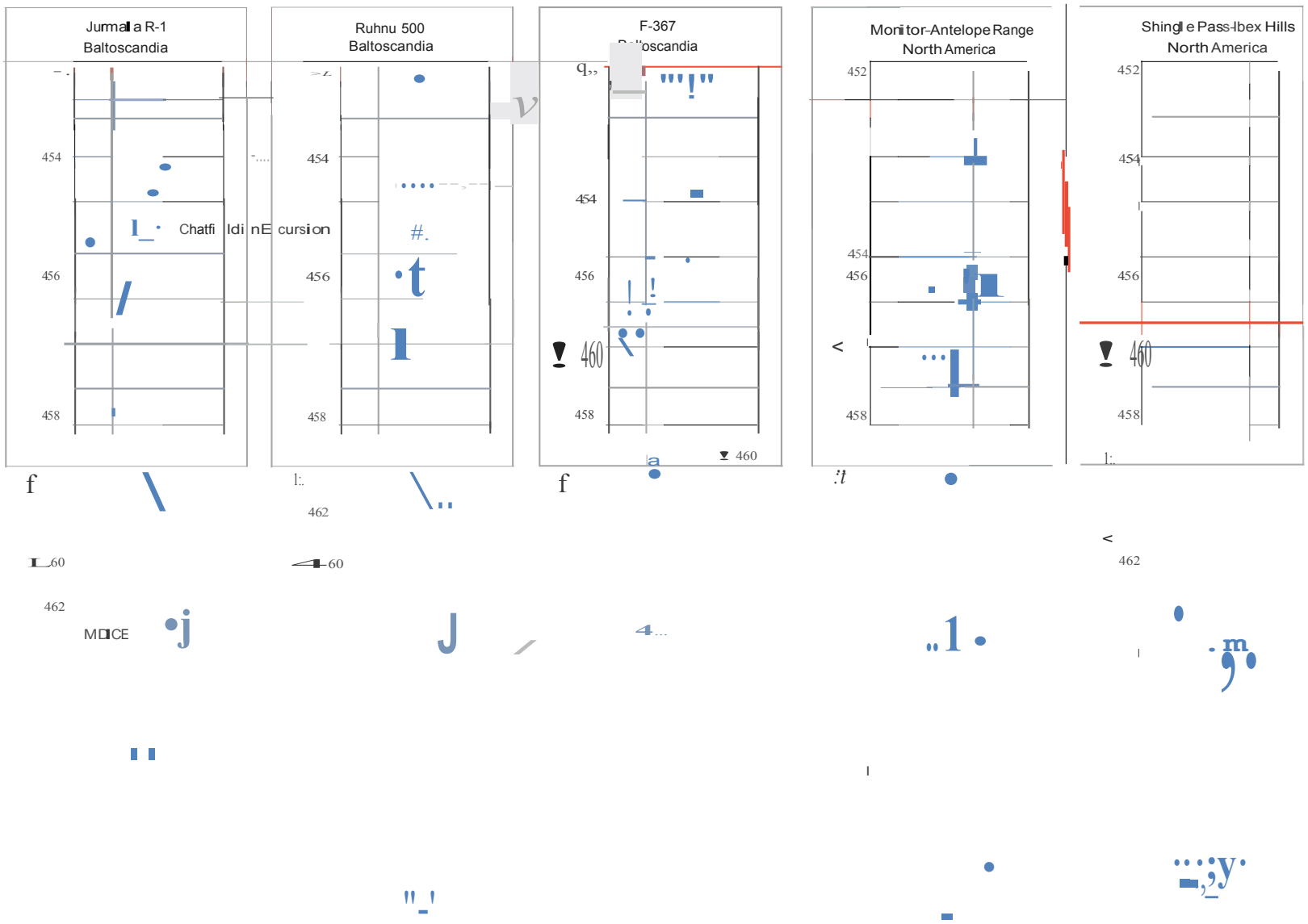
Jurmala R-1
Baltoscandia
Ruhnu 500
Baltoscandia
F-367
Monitor-Antelope Range
North America
Shingle Pass-Ibex Hills
North America
454
456
458
460
462
452

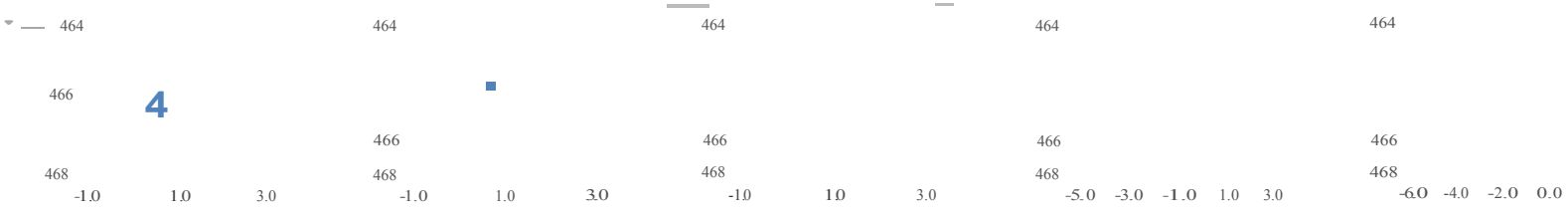
464
466
468
-1.0
1.0
3.0
4
464
466
468
-1.0
1.0
3.0
464
466
468
-1.0
1.0
3.0
464
466
468
-5.0
-3.0
-1.0
1.0
3.0
464
466
468
-6.0
-4.0
-2.0
0.0

w

Figure 5

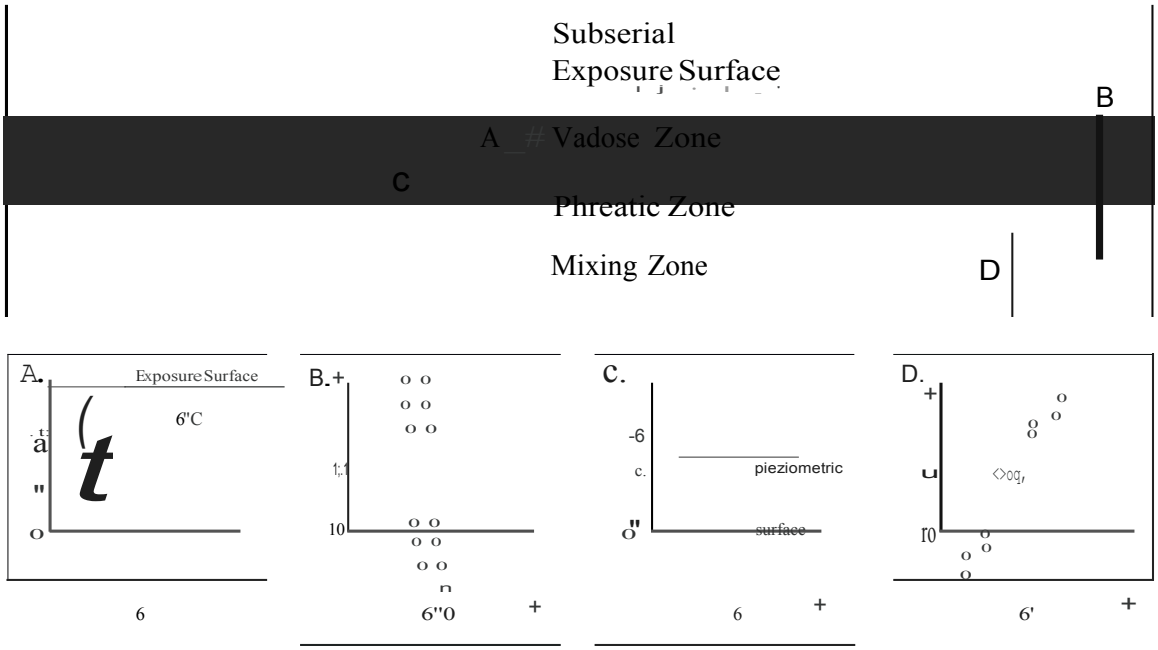
Subserial
Exposure Surface
B
A
Vadose Zone
C
Phreatic Zone
Mixing Zone
D
A.
Exposure Surface
6"C
B.+
10
C.
-6
pieziometric
surface
D.
+
6
6''0
+
6
+
6'
+

Figure 6

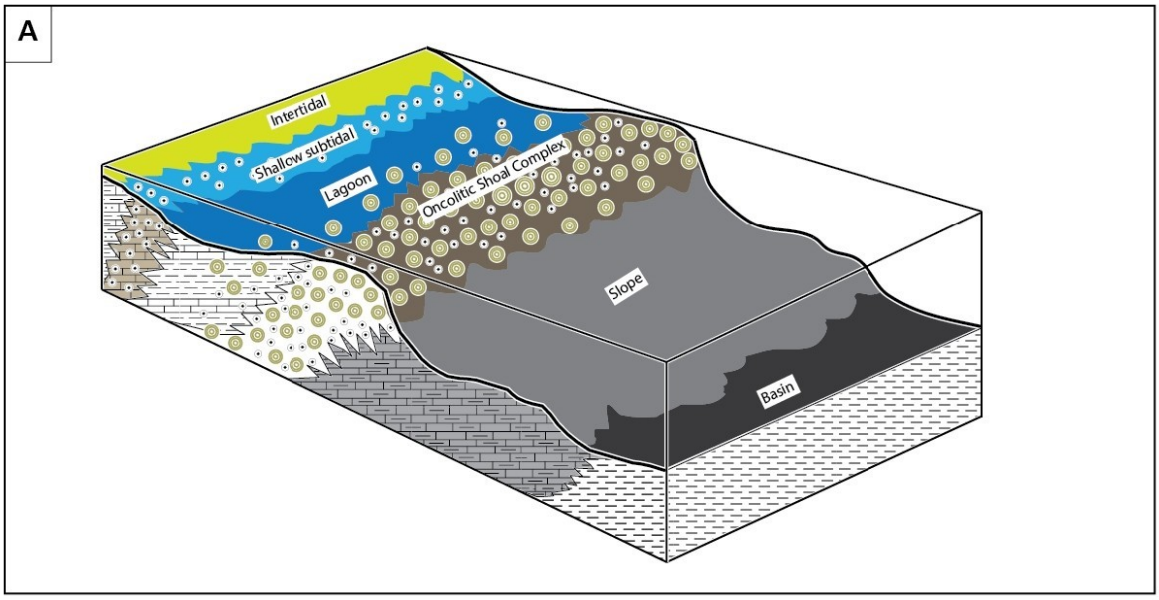
A
Intertidal
Shallow subtidal
Lagoon
Oncolitic Shoal Complex
Slope
Basin

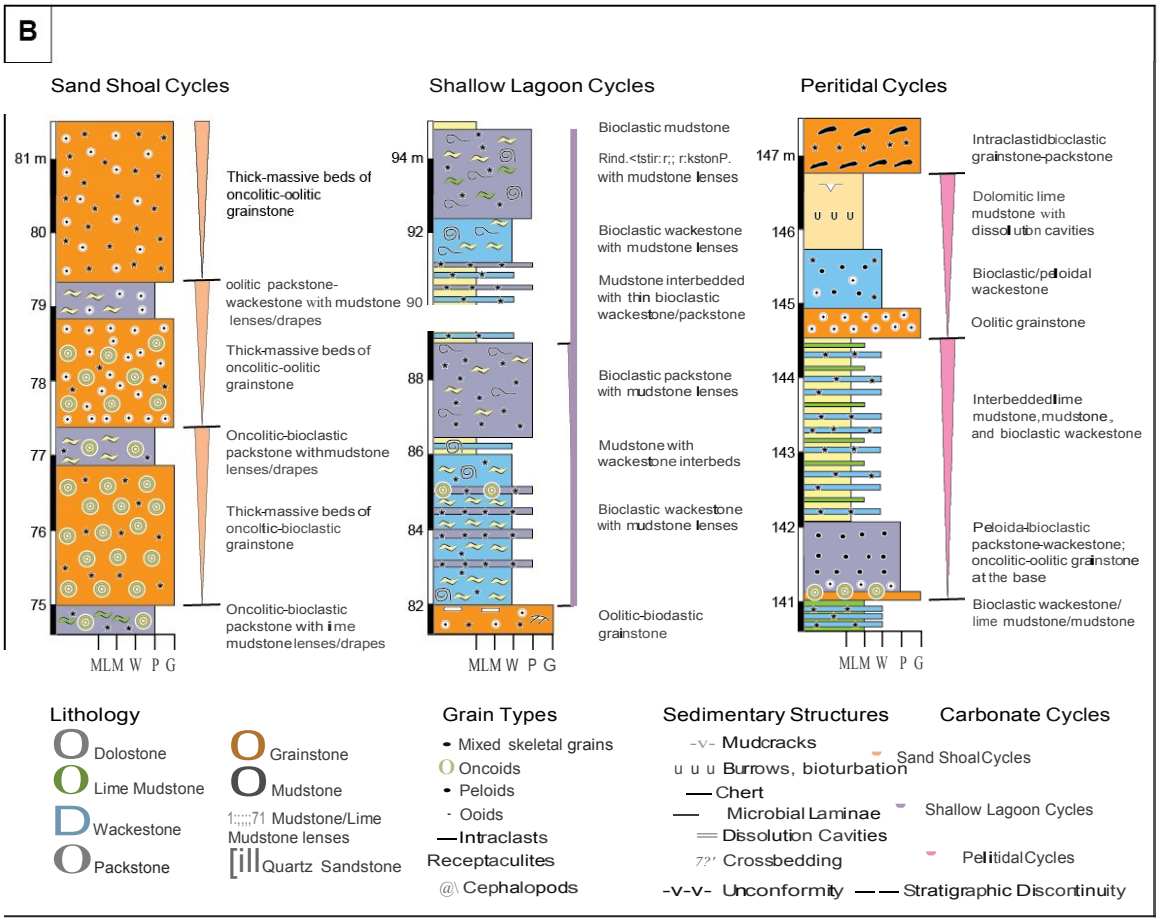
B
Sand Shoal Cycles
81 m
80
79
78
77
76
75
Thick-massive beds of oncolitic-oolitic grainstone
oolitic packstone-wackestone with mudstone lenses/drapes
Thick-massive beds of oncolitic-oolitic grainstone
Oncolitic-bioclastic packstone withmudstone lenses/drapes
Thick-massive beds of oncolitic-bioclastic grainstone
Oncolitic-bioclastic packstone with lime mudstone lenses/drapes
MLM W P G
Shallow Lagoon Cycles
94 m
92
90
88
86
84
82
Bioclastic mudstone
Rind.<tstir:r;; r:kstonP. with mudstone lenses
Bioclastic wackestone with mudstone lenses
Mudstone interbedded with thin bioclastic wackestone/packstone
Bioclastic packstone with mudstone lenses
Mudstone with wackestone interbeds
Bioclastic wackestone with mudstone lenses
Oolitic-biodastic grainstone
MLM W P G
Peritidal Cycles
147 m
146
145
144
143
142
141
Intraclastidbioclastic grainstone-packstone
Dolomitic lime mudstone with dissolution cavities
Bioclastic/peloidal wackestone
Oolitic grainstone
Interbeddedlime mudstone, mudstone, and bioclastic wackestone
Peloidal-bioclastic packstone-wackestone; oncolitic-oolitic grainstone at the base
Bioclastic wackestone/ lime mudstone/mudstone
MLM W P G
Lithology
Dolostone
Lime Mudstone
Wackestone
Packstone
Grainstone
Mudstone
1:;;;;71 Mudstone/Lime Mudstone lenses
Quartz Sandstone
Grain Types
Mixed skeletal grains
Oncoids
Peloids
Ooids
Intraclasts
Receptaculites
Cephalopods
Sedimentary Structures
Mudcracks
Burrows, bioturbation
Chert
Microbial Laminae
Dissolution Cavities
Crossbedding
Unconformity
Carbonate Cycles
Sand Shoal Cycles
Shallow Lagoon Cycles
Pelitidal Cycles
Stratigraphic Discontinuity

Figure 7

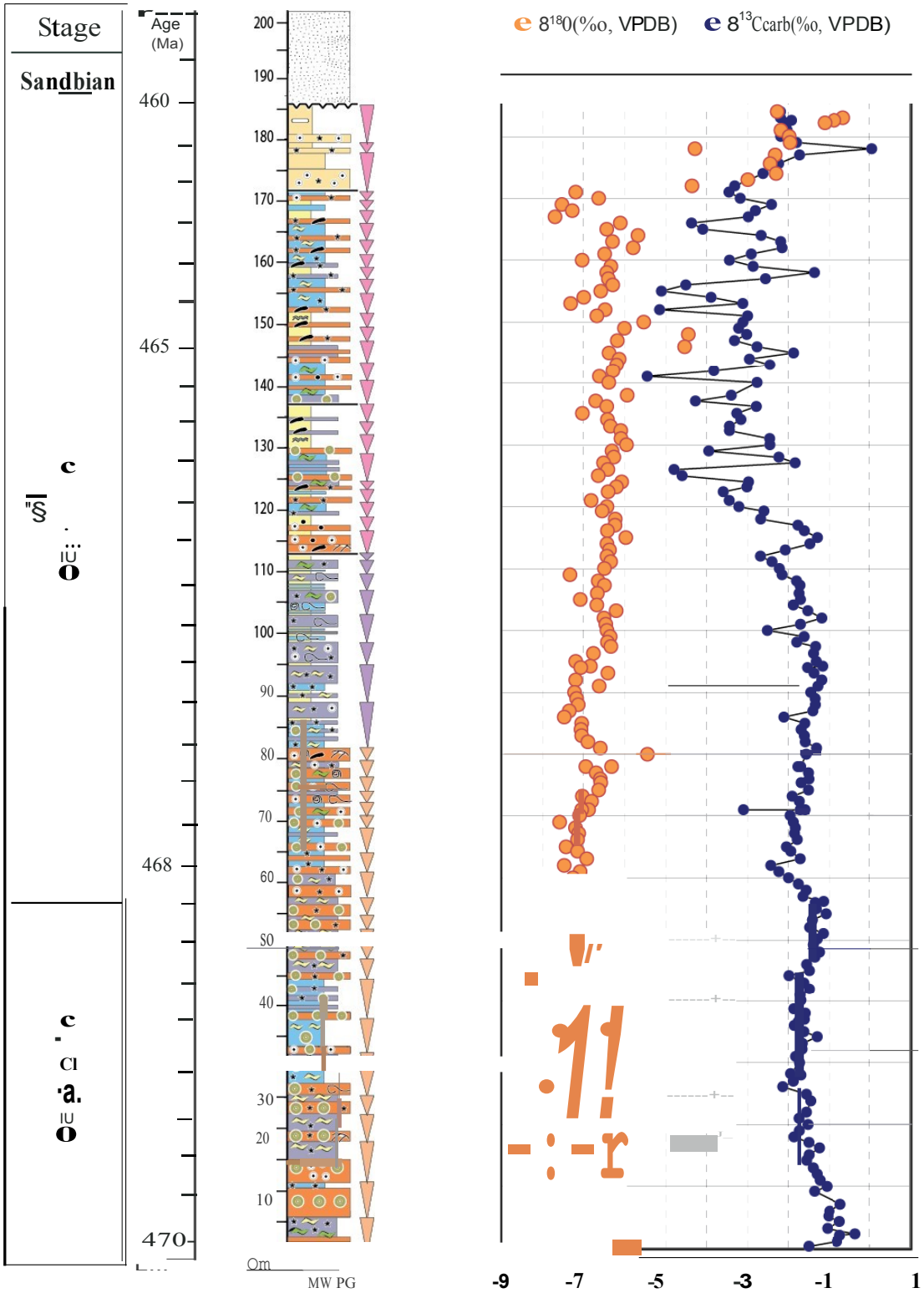
Stage
Age (Ma)
Sandbian
460
465
468
470
200
190
180
170
160
150
140
130
120
110
100
90
80
70
60
50
40
30
20
10
0m
MW PG
δ18O(‰, VPDB)
δ13Ccarb(‰, VPDB)
-9
-7
-5
-3
-1
1

Figure 8

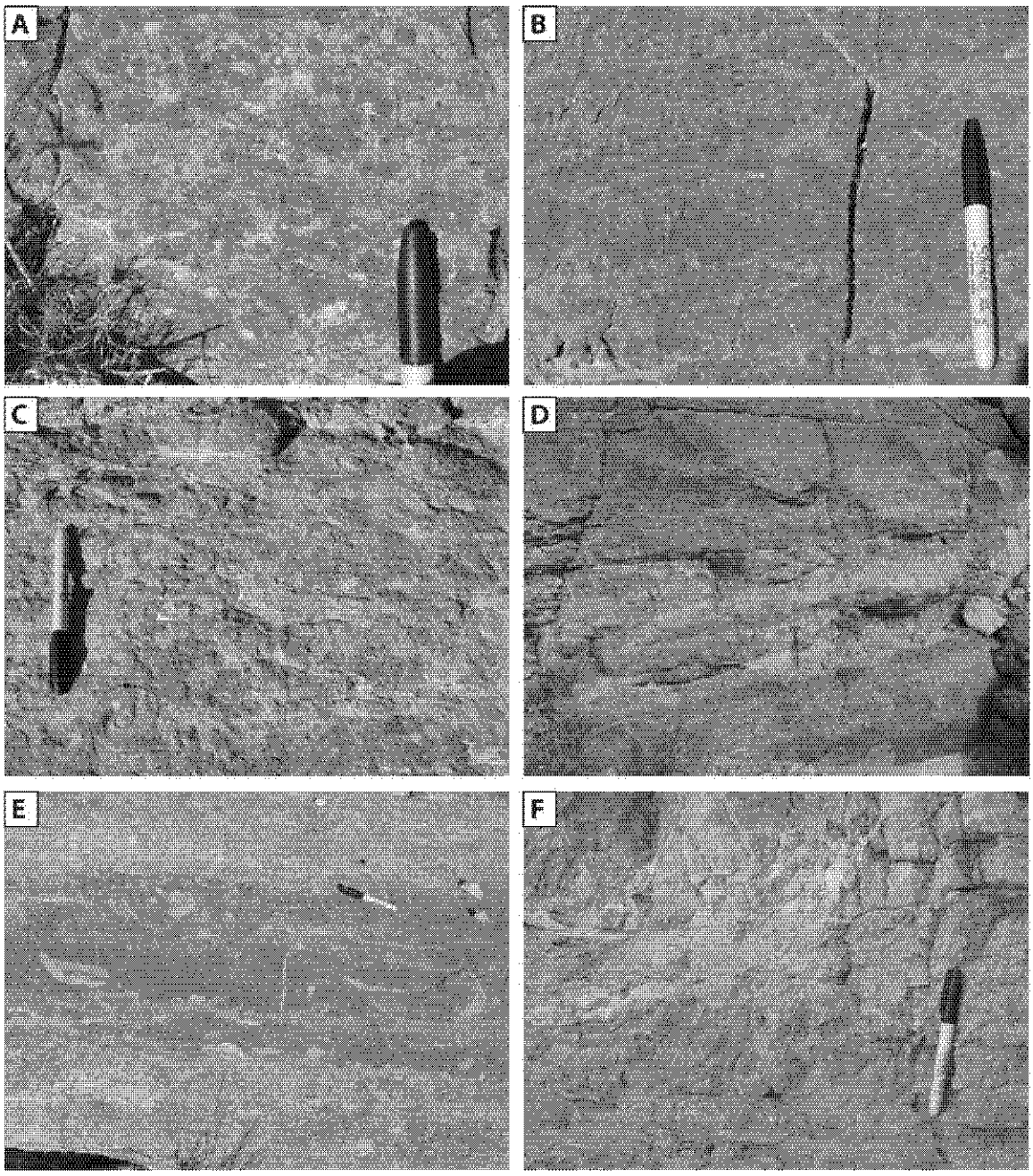

Figure 9

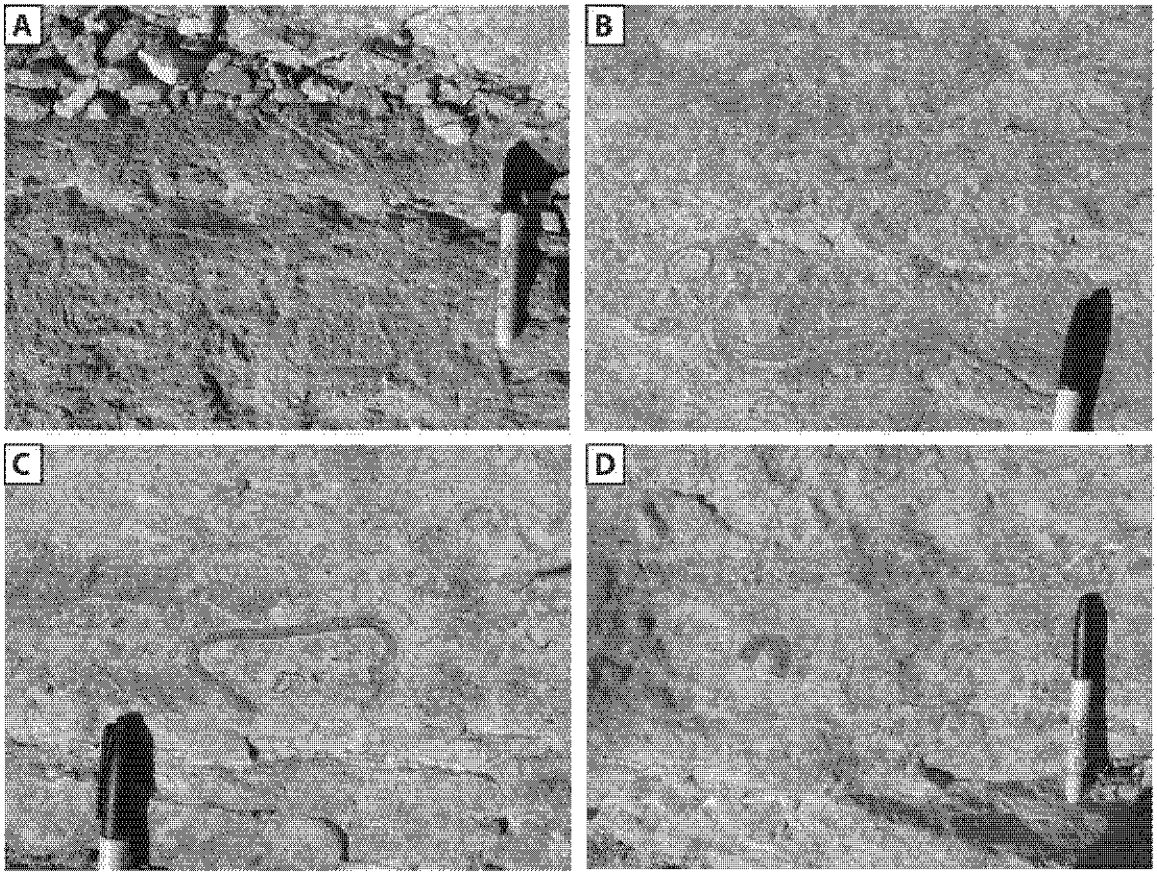

Figure 10

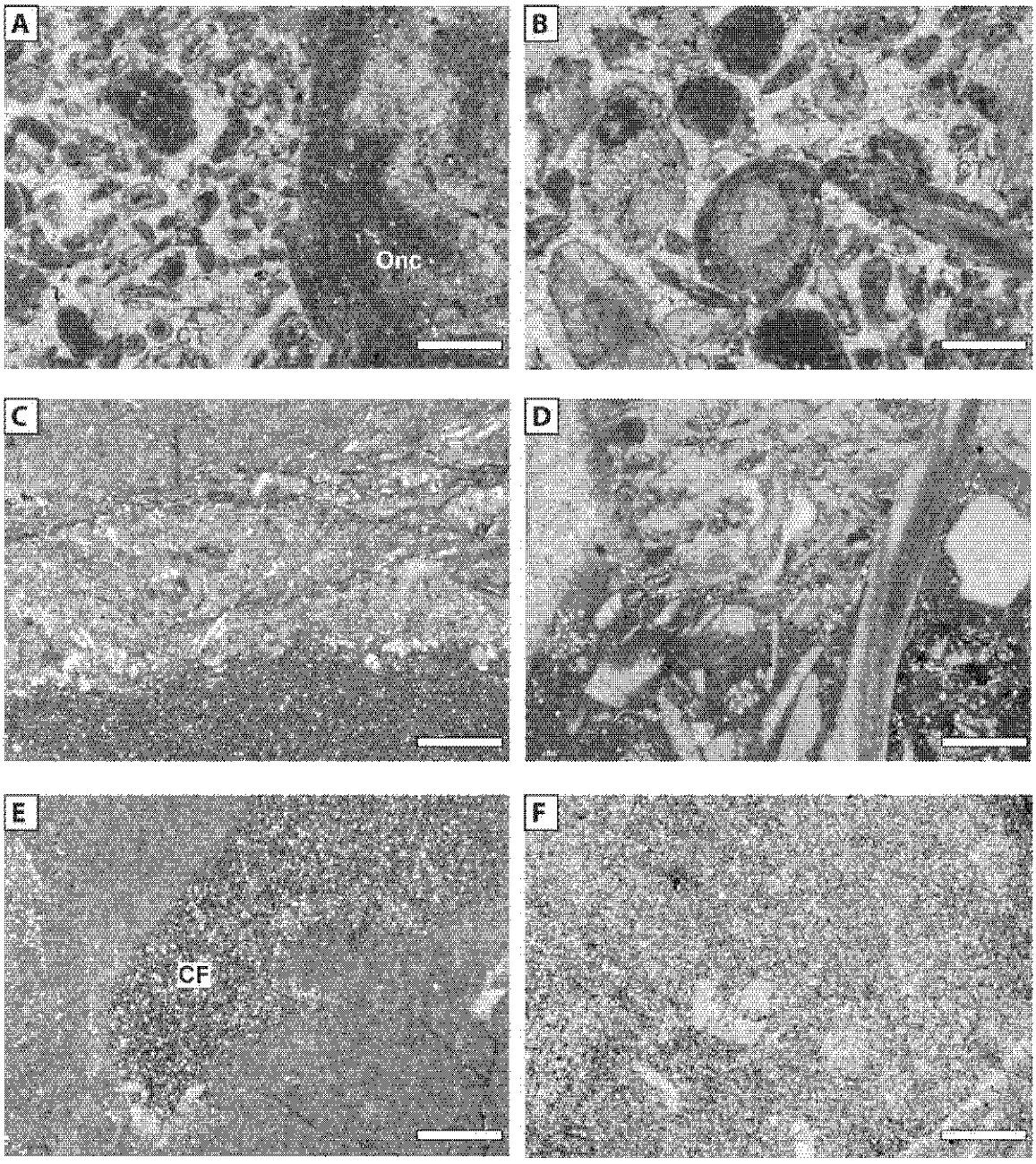

Figure 11

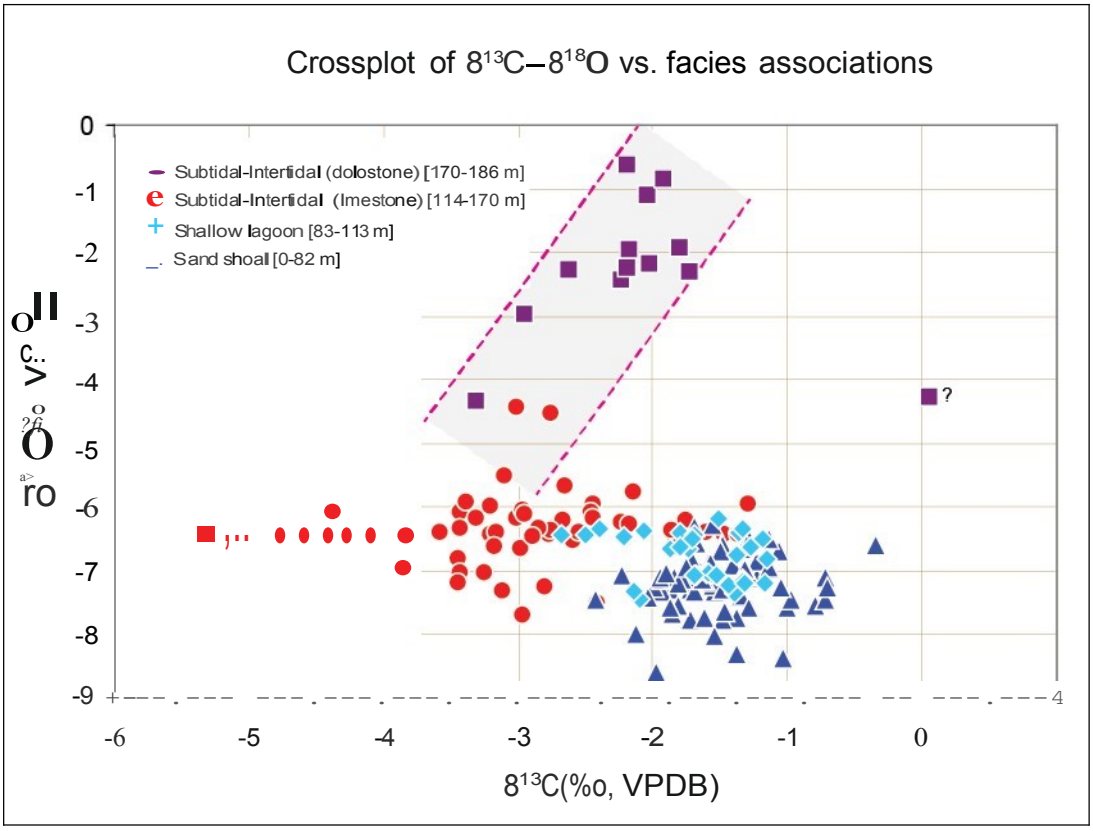
Crossplot of δ13C–δ18O vs. facies associations
Subtidal-Interfidal (dolostone) [170-186 m]
Subtidal-Interfidal (limestone) [114-170 m]
Shallow lagoon [83-113 m]
Sand shoal [0-82 m]
0
-1
-2
-3
-4
-5
-6
-7
-8
-9
-6
-5
-4
-3
-2
-1
0
δ13C(‰, VPDB)

Figure 12

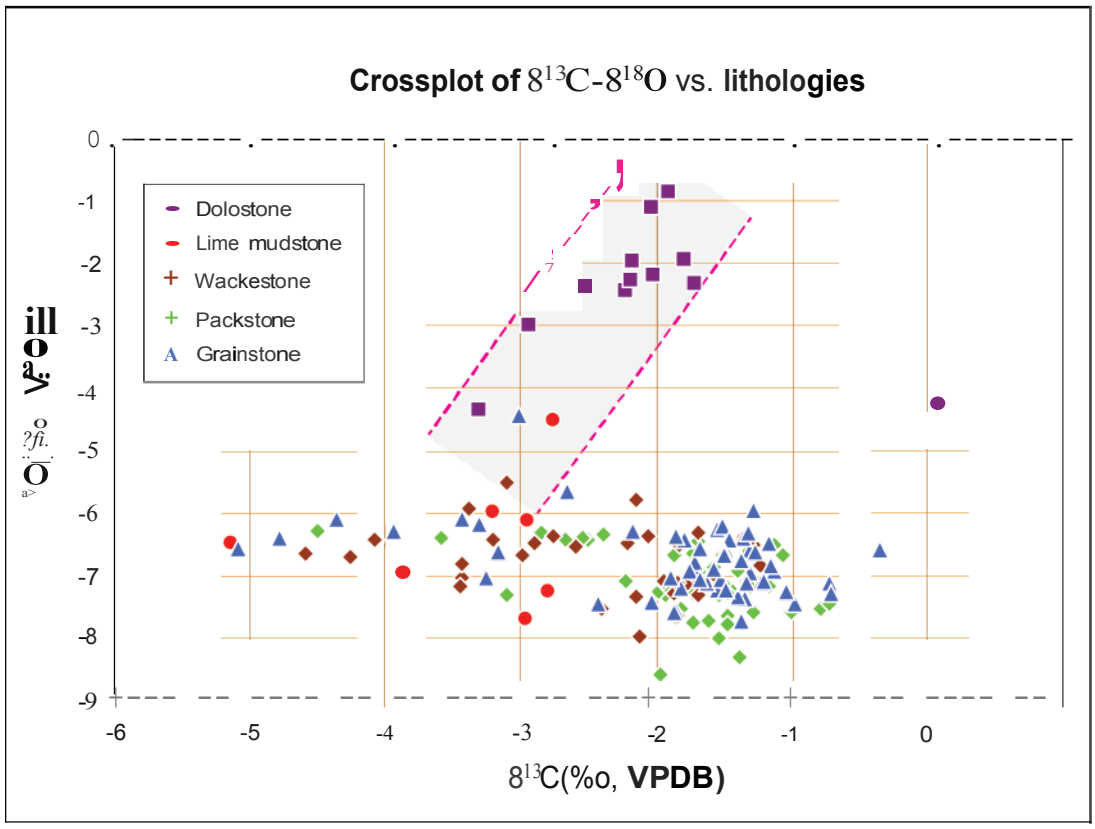
Crossplot of δ13C-δ18O vs. lithologies
Dolostone
Lime mudstone
Wackestone
Packstone
Grainstone
0
-1
-2
-3
-4
-5
-6
-7
-8
-9
-6
-5
-4
-3
-2
-1
0
δ13C(‰, VPDB)

Figure 13

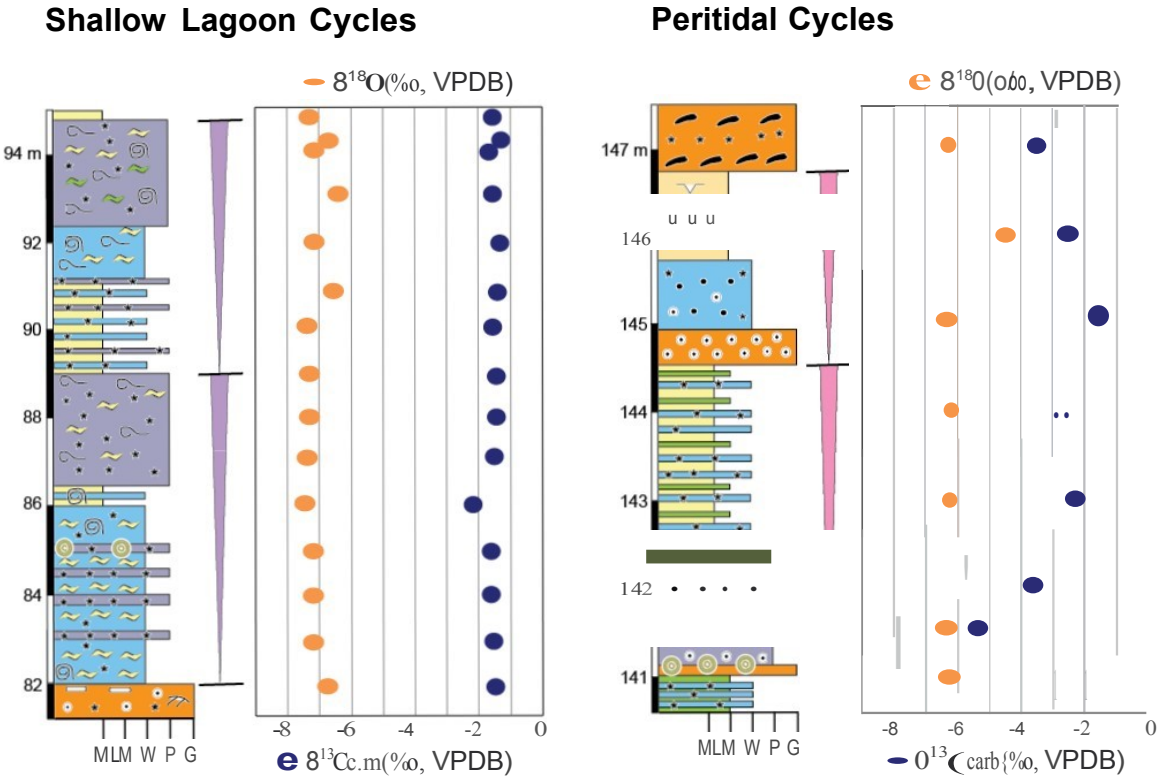
Shallow Lagoon Cycles
Peritidal Cycles
δ18O(‰, VPDB)
δ13Cc.m(‰, VPDB)
δ18O(‰, VPDB)
δ13Ccarb(‰, VPDB)
94 m
92
90
88
86
84
82
147 m
146
145
144
143
142
141
MLM W P G
-8
-6
-4
-2
0

Figure 14

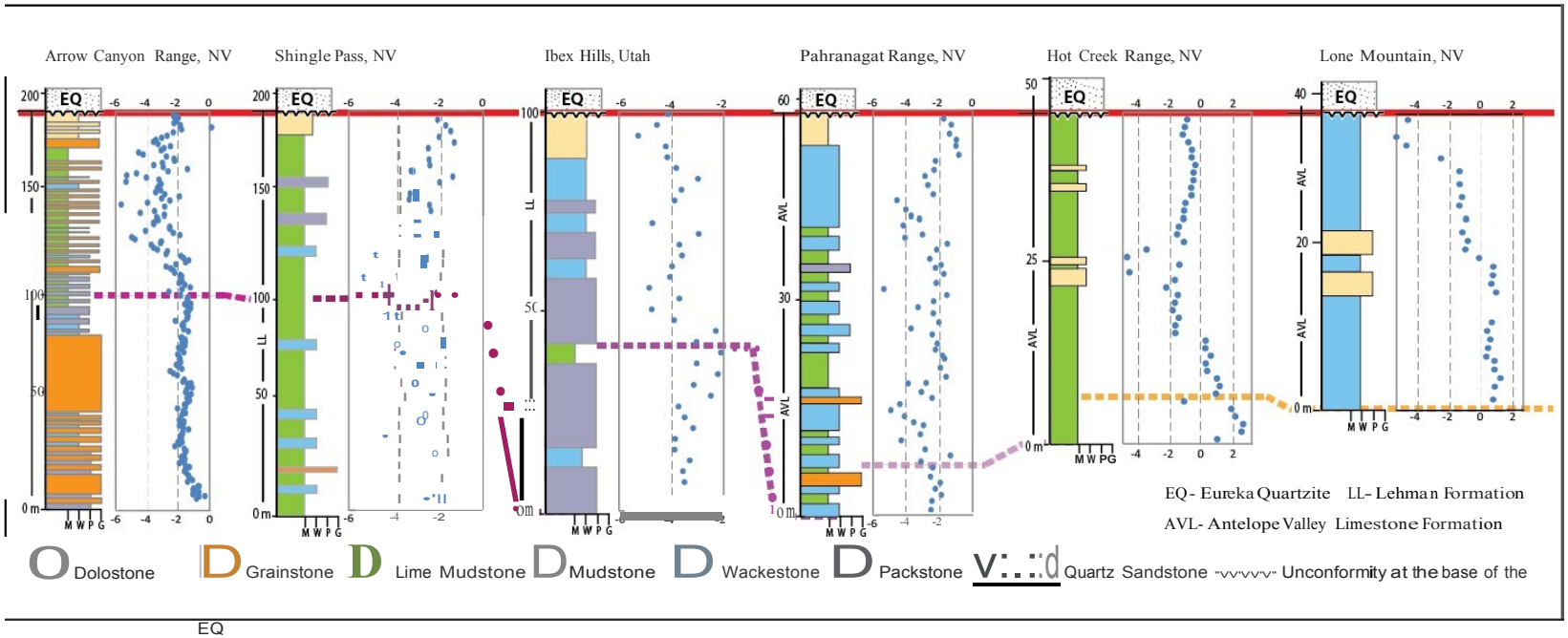
Arrow Canyon Range, NV
Shingle Pass, NV
Ibex Hills, Utah
Pahranagat Range, NV
Hot Creek Range, NV
Lone Mountain, NV
EQ
LL
AVL
MWPG
EQ- Eureka Quartzite LL- Lehman Formation
AVL- Antelope Valley Limestone Formation
Dolostone
Grainstone
Lime Mudstone
Mudstone
Wackestone
Packstone
Quartz Sandstone
Unconformity at the base of the

EQ

Figure 15

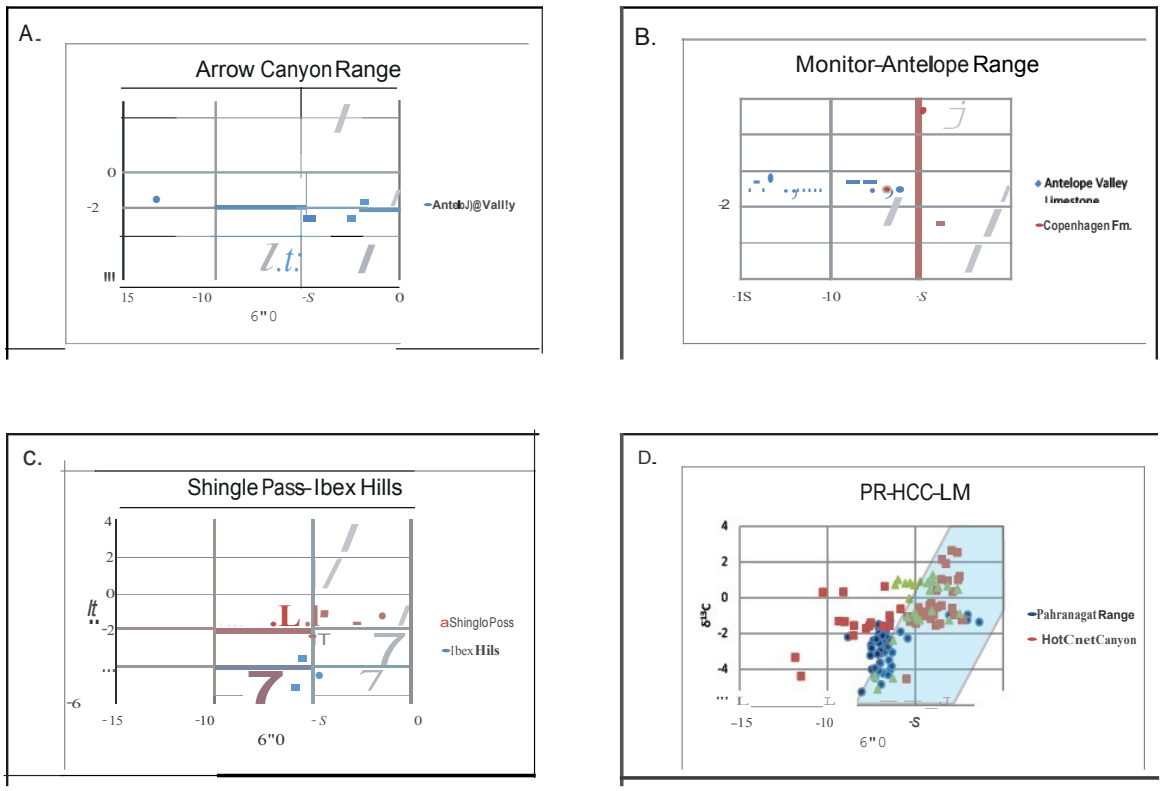
A.
Arrow Canyon Range
0
-2
15
-10
-S
0
6"0
B.
Monitor-Antelope Range
-2
-10
-S
Antelope Valley
Copenhagen Fm.
C.
Shingle Pass-Ibex Hills
4
2
0
-2
-6
-15
-10
-S
0
6"0
aShingloPoss
Ibex Hils
D.
PR-HCC-LM
4
2
0
-2
-4
-15
-10
-S
6"0
Pahranagat Range
HotCnetCanyon

BIBLIOGRAPHY

Ainsaar, L., Kaljo, D., Martma, T., Meidla, T., Mannik, P., Nolvak, J., and Tinn, O., 2010, Middle and Upper Ordovician carbon isotope chemostratigraphy in Baltoscandia: A correlation standard and clues to environmental history: Palaeogeography, Palaeolclimatology, Palaeoecology, v.294, p.189-201.

Albanesi, G.L., Bergstrom, S.M., Schmitz, B., Serra, F., Feltes, N.A., Voldman, G.G., and Ortega, G., 2013, Darriwilian (Middle Ordovician) $\delta^{13}C_{Carb}$ chemostratigraphy in the Precordillera of Argentina: Documentation of the middle Darriwilian Isotope Carbon Excursion (MDICE) and its use for intercontinental correlation: Palaeogeography, Palaeolclimatology, Palaeoecology, v.389, p. 48-63.

Allan, J.R., and Matthews, R.K., 1982, Isotope Signatures Associated with Early Meteoric Diagenesis: Sedimentology, v. 29, p. 797-818.

Bergström, S.M., Lehnert, O., Calner, M., and Joachimski, M.M., 2012, A new upper MiddleOrdovician–Lower Silurian drillcore standard succession from Borenshult in Östergötland, southern Sweden: 2. Significance of δ13C chemostratigraphy: GFF, v. 134, p. 39-63.

Brasier, M.D., Corfield, R.M., Derry, L.A., Rozanov, A.Y., and Zhuravlev, A.Y., 1994, Multiple $\delta^{13}C$ excursions spanning the Cambrian explosion to the Botomian crisis in Siberia: Geology, v. 22, p. 455-458.

Burkhard, M., 1993, Calcite twins, their geometry, appearance and significance as stress-strain markers and indicators of tectonic regime: a review: Journal of Structural Geology, v. 15, p. 351-368.

Calner, M., Lehnert, O.,Wu, R., Dahlqvist, P., and Joachimski, M., 2014, δ ^{13}C chemostratigraphy in the Lower–Middle Ordovician succession of Öland (Sweden) and the global significance of the MDICE: GFF, v. 136:1, p. 48-54.

Cooper, J.D., and Keller, M., 2001, Palaeokarst in the Ordovician of the southern Great Basin, USA: implications for sea-level history: Sedimentology, v. 48, p.855-873.

Derry, L.A., 2010, A burial diagenesis origin for the Ediacaran Shuram-Wonoka carbon isotope anomaly: Earth and Planetary Science Letters, v. 294, p. 152-162.

Derry, L.A., 2010, On the significance of δ^{13}C correlations in ancient sediments: Earth and Planetary Science Letters, v. 296, p. 497-501.

Druschke, P.A., Jiang, G., Anderson, T.B., and Hanson, A.D., 2009, Stromatolites in the Late Ordovician Eureka Quartzite: implications for microbial growth and preservation in siliciclastic settings: Sedimentology, v. 56, p. 1275-1291.

Edwards, C.T., and Saltzman, M.R., 2014, Carbon isotope (δ^{13}Ccarb) stratigraphy of the Lower–Middle Ordovician (Tremadocian–Darriwilian) in the Great Basin,

western United States: Implications for global correlation: Palaeogeography, Palaeoclimatology, Palaeoecology v. 399, p. 1–20.

Fike, D.A., Grotzinger, J.P., Pratt, L.M., and Summons, R.E., 2006, Oxidation of the Ediacaran Ocean: Nature, v. 444, p. 744-747.

Grotzinger, J.P., Fike, D.A., and Fischer, W.W., 2011, Enigmatic origin of the largest-known carbon isotope excursion in Earth's history: Nature, v. 4, p. 285-292.

Gunn, S.M., 1998, Paleoenvironment and paleoecology of the Ordovician Pogonip Group Member F (Arrow Canyon Range, south-central Nevada); implications for the early Paleozoic history of gastropods and bivalves: California, University of California at Riverside, unpublished Master's thesis, p. 1-143.

Halverson, G.P., Hoffman, P.F., Schrag, D.P., Maloof, A.C., and Rice, A.H.N., 2005, Toward a Neoproterozoic composite carbon-isotope record: Geological Society of America Bulletin, v. 117, p. 1181-1207.

Hoffman, P.F., Kaufman, A.J., Halverson, G.P., and Schrag, D.P., 1998, A Neoproterozoic Snowball Earth: Science, v. 281, p. 1342-1346.

Jacobsen, S.B., and Kaufman, A.J., 1999, The Sr, C and O isotopic evolution of Neoproterozoic seawater: Chemical Geology, v. 161, p. 37-57.

Jiang, G., Christie-Blick, N., Kaufman, A.J., Banerjee, D.M., and Rai, V., 2002, Sequence stratigraphy of the Neoproterozoic Infra Krol Formation and Krol Group, Lesser Himalaya, India: Journal of Sedimentary Research, vol. 72, p. 524-542.

Jiang, G., Kaufman, A.J., Christie-Blick, N., Zhang, S., and Wu, H., 2007, Carbon isotope variability across the Ediacaran Yangtze platform in South China: Implications for a large surface-to-deep ocean $\delta^{13}C$ gradient: Earth and Planetary Science Letters, v. 261, p. 303-320.

Jiang, G., Zhang, S., Shi, X., and Wang, X., 2008, Chemocline instability and isotope variations of the Ediacaran Doushantuo basin in South China: Science in China Series D-Earth Sciences, v. 51, p. 1560-1569.

Jiang, G., Shi, X., Zhang, S., Wang, Y., and Xiao, S., 2011, Stratigraphy and paleogeography of the Ediacaran Doushantuo Formation (ca. 635-551 Ma) in South China: Gondwana Research, v. 19, p. 831-849.

Johnston, D.T., Macdonald, F.A., Gill, B.C., Hoffman, P.F., and Schrag, D.P., 2012, Uncovering the Neoproterozoic Carbon Cycle: Nature, v. 483, p. 320-323.

Kaufman, A.J., Hayes, J.M., Knoll, A.H., and Germs, G.J.B., 1991, Isotopic compositions of carbonates and organic carbon from upper Proterozoic

successions in Namibia; stratigraphic variation and the effects of diagenesis and metamorphism: Precambrian Research, v. 49, p. 301-327.

Kaufman, A.J., and Knoll, A.H., 1995, Neoproterozoic variations in the C-isotopic composition of seawater; stratigraphic and biogeochemical implications: Precambrian Research, v. 73, p. 27-49.

Kaufman, A.J., Jiang, G., Christie-Blick, N., Banerjee, D. and Rai, V., 2006, Stable isotope record of the terminal Neoproterozoic Krol platform in the Lesser Himalayas of northern India: Precambrian Research, v. 147, p. 156–185.

Knauth, L.P., and Kennedy, M.J., 2009, The late Precambrian greening of the Earth: Nature, v. 460, p. 728-732.

Knoll, A.H., Hayes, J.M., Kaufman, A.J., Swett, K., and Lambert, I.B., 1986, Secular variation in carbon isotope ratios from upper Proterozoic successions of Svalbard and East Greenland: Nature, v. 321, p. 832-838.

Kosmidis, A.P., 2009, Sequence and chemostratigraphic study across the basal Eureka Quartzite unconformity in the Great Basin, Nevada: implications for the origin of the Late Ordovician carbon isotope excursion: Nevada, University of Nevada-Las Vegas, unpublished Master's thesis, p.1-100.

Kump, L.R., Arthur, M.A., Patzkowsky, M.E., Gibbs, M.T., Pinkus, D.S., and Sheehan, P.M., 1999, A weathering hypothesis for glaciation at high atmospheric pCO_2 during the Late Ordovician: Paleogeography, Paleoclimatology, Paleoecology, v. 152, p. 173-187.

Langenheim, R.L., Carss, B.W., Kennerly, J.B., McCutcheon, V.A., and Waines, R.H., 1962, Paleozoic section in Arrow Canyon Range, Clark County, Nevada: AAPG Bulletin, v. 46, p. 592-609.

Lu, M., Zhu, M., Zhang, J., Shields-Zhou, G., Li, G., Zhao, F., Zhao, J., and Zhao, M., 2013, The DOUNCE event at the top of the Ediacaran Doushantuo Formation, South China: Broad stratigraphic occurrence and non-diagenetic origin: Precambrian Research, v. 225, p. 86-109.

Melezhik, V.A., Gorokhov, I.M., Kuznetsov, A.B., and Fallick, A.E., 2001, Chemostratigraphy of Neoproterozoic Swart, P.K., 2008, Global synchronous changes in the carbon isotopic composition of carbonate sediments unrelated to changes in the global carbon cycle: Proceedings of the National Academy of Sciences, v. 105, p. 13741-13745.

Metzger, J.G., and Fike, D.A., 2013, Techniques for assessing spatial heterogeneity of carbonate $\delta^{13}C$ values: Implications for craton-wide isotope gradients: Sedimentology v. 60, p. 1405-1431.

Munnecke, A., Calner, M., Harper, D.A.T., and Servais, T., 2010, Ordovician and Silurian sea-water chemistry, sea-level, and climate: A synopsis: Paleogeography, Paleoclimatology, Paleoecology, v. 296, p. 389-413.

Myrow, P.M. et al., 2013, Latest Devonian (Famennian) global events in western Laurentia: Variations in the carbon isotopic record linked to diagenetic alteration below regionally extensive unconformities: Paleogeography, Paleoclimatology, Paleoecology, v. 386, p. 194-209.

Oehlert, A.M., and Swart, P.K., Interpreting carbonate and organic carbon isotope covariance in the sedimentary record: Nature Communications, v. 5, article 4652.

Panchuk, K.M., Holmden, C.E., and Leslie, S.A., 2006, Local Controls on Carbon Cycling in the Ordovician Midcontinent Region of North America, with Implications for Carbon Isotope Secular Curves: Journal of Sedimentary Research, v. 76, p. 200-211.

Patterson, W.P., and Walter, L.M., 1994, Depletion of ^{13}C in seawater $\Sigma C0_2$ on modern carbonate platforms: Significance for the carbon isotopic record of carbonates: Geology, v. 22, p. 885-888.

Paulsen, T.S., Demosthenous, C.M., Myrow, P.M., Hughes, N.C., and Parcha, S.K., 2007, Paleostrain stratigraphic analysis of calcite twins across the Cambrian-Ordovician unconformity in the Tethyan Himalaya, Spiti and Zanskar valley regions, India: Journal of Asian Earth Sciences, v. 31, p. 44-54.

Rosenbaum, J., Sheppard, S.M.F., 1986, An isotopic study of siderites, dolomites and ankerites at high temperatures: Geochimica Cosmochimica Acta, v.50, p.1147–1150.

Ross, R.J. Jr., 1996, Quintessesnce of the Ordovician: From Rocky Mountain Beaches to the Depths of Nevada: Society for Sedimentary Geology, Rocky Mountain Section, v.1996, p. 47-62.

Saltzman, M.R., Runnegar, B., and Lohmann, K.C., 1998, Carbon isotope stratigraphy of Upper Cambrian (Steptoean Stage) sequences of the eastern Great Basin; record of a global oceanographic event: Geological Society of America Bulletin, v. 110, p. 285-297.

Saltzman, M.R., 2005, Long-lived glaciation in the Late Ordovician? Isotopic and sequence-stratigraphic evidence from western Laurentia: Geology, v. 33, p. 109-112.

Scotese, C.R., McKerrow, W.S., 1990. Revised world maps and introduction: Geological Society of London Memoirs 12, 1–21.

Stricker, G.D., and Carozzi, A.V., 1973, Carbonate Microfacies of the Pogonip Group (Lower Ordovician) Arrow Canyon Range, Clark County, Nevada, USA: Bulletin Centre Recherche Pau (SNPA), v. 30, p. 499-541.

Swart, P.K., 2008, Global synchronous changes in the carbon isotopic composition of carbonate sediments unrelated to changes in the global carbon cycle: Proceedings of the National Academy of Sciences, v. 105, p. 13741-13745.

Swart, P.K., Reijmer, J.J., and Otto, R., 2009, A re-evaluation of facies on Great Bahama Bank II: Variations in the $\delta^{13}C$, $\delta^{18}O$ and mineralogy of surface sediments, in Swart, P.K., et al., eds., Perspectives in carbonate geology: A tribute to the career of Robert Nathan Ginsburg: International Association of Sedimentologists Special Publication 41, p. 47-60.

Swart, P.K., and Kennedy, M.J., 2012, Does the global stratigraphic reproducibility of δ13C in Neoproterozoic carbonates require a marine origin? A Pliocene-Pleistocene comparison: Geology, v. 40, p. 87-90.

Thompson, C.K., and Kah, L.C., 2011, Sulfur isotope evidence for widespread euxinia and fluctuating oxycline in Early to Middle Ordovician greenhouse oceans: Palaeogeography, Palaeoclimatology, Palaeoecology, v.313, p. 189-214.

Wang, W., Zhou, C., Guan, C., Yuan, X., Chen, Z., and Wan, B., 2014, An integrated carbon, oxygen, and strontium isotopic studies of the Lantian Formation in South China with implications for the Shuram anomaly: Chemical Geology, v. 373, p. 10-26.

Zhu, M., Zhang, J., and Yang, A., 2007, Integrated Ediacaran (Sinian) chronostratigraphy of South China: Palaeogeography, Palaeoclimatology, Palaeoecology, v. 254, p. 7-61.

Zhu, M., Lu, M., Zhang, J., Zhao, F., Li, G., Yang, A., Zhao, X., and Zhao, M., 2013, Carbon isotope chemostratigraphy and sedimentary facies evolution of the Ediacaran Doushantuo Formation in western Hubei, South China: Precambrian Research, v. 225, p. 7-28.

VITA

Graduate College
University of Nevada, Las Vegas

Patricia Suzanne Williams

Degrees:
Bachelor of Science, Geology and Geophysics, 2012
Missouri University of Science and Technology

Special Honors and Awards:
Bernada French Award
E. Edwards & M. Olswang Scholarship
Graduate & Professional Student Association Research Grant

Thesis Title: Carbon Isotope Variations Associated with a Middle Ordovician Karstic Unconformity

Thesis Examination Committee: Chairperson,
Ganqing Jiang, Ph. D. Committee Member,
Terry L. Spell, Ph. D. Committee Member,
Minghua Ren, Ph. D.
Graduate Faculty Representative, Brian P. Hedlund, Ph. D.